Contrasted microbial community colonization of a bauxite residue deposit marked by a complex geochemical context

Luis Alberto Macías-Pérez, Clément Levard, Mohamed Barakat, Bernard Angeletti, Daniel Borschneck, Laurent Poizat, Wafa Achouak, Melanie Auffan

HAL Id: hal-03468413

https://cnrs.hal.science/hal-03468413

Submitted on 16 Dec 2021

1 ***"Contrasted Microbial community colonization of a bauxite residue deposit***

2 ***marked by a complex geochemical context."***

3 Luis Alberto Macías-Pérez [a,b], Clément Levard [a], Mohamed Barakat [b], Bernard

4 Angeletti [a], Daniel Borschneck [a], Laurent Poizat [d], Wafa Achouak [b*], Mélanie Auffan [a,c*]

5 *These authors contributed equally to the study

6 **Author contact information (FAMILY NAME, Name):**

7 1) MACÍAS-PÉREZ, Luis Alberto [a,b] (Corresponding author)
8 Address: CEREGE, Technopôle de l'Arbois-Méditerranée, BP80, 13545 Aix-en-
9 Provence, France
10 Email: macias@cerege.fr
11 Telephone number: +33 766887887 (France)
12 Fax: +33 (0)4 13 94 91 30 (France)
13 2) LEVARD, Clément [a]
14 Email: levard@cerege.fr
15 3) BARAKAT, Mohamed [b]
16 Email: mohamed.barakat@cea.fr
17 4) ANGELETTI, Bernard [a]
18 Email: angeletti@cerege.fr
19 5) BORSCHNECK, Daniel [a]
20 Email: borschneck@cerege.fr
21 6) POIZAT, Laurent [d]
22 Email: laurent.poizat@alteo-alumina.com
23 7) ACHOUAK, Wafa [b]
24 Email: wafa.achouak@cea.fr
25 8) AUFFAN, Mélanie [a,c]
26 Email: auffan@cerege.fr
27

28 **Author affiliations:**

29 a. Aix Marseille Université, CNRS, IRD, INRAE, Collège de France, CEREGE,
30 13545, Aix-en-Provence, France
31 b. Aix Marseille Univ, CEA, CNRS, BIAM, LEMIRE, Laboratory of Microbial Ecology
32 of the Rhizosphere, ECCOREV FR 3098, F-13108, St-Paul-lez-Durance, France
33 c. Civil and Environmental Engineering, Duke University, Durham, NC 27708, USA
34 d. ALTEO Alumina, 13120, Gardanne, France
35

38

Abstract

Bauxite residue is the alkaline byproduct generated during alumina extraction and is commonly landfilled in open-air deposits. The growth in global alumina production have raised environmental concerns about these deposits since no large-scale reuses exist to date. Microbial-driven techniques including bioremediation and critical metal bio-recovery are now considered sustainable and cost-effective methods to revalorize bauxite residues. However, the establishment of microbial communities and their active role in these strategies are still poorly understood. We thus determined the geochemical composition of different bauxite residues produced in southern France and explored the development of bacterial and fungal communities using Illumina high-throughput sequencing. Physicochemical parameters were influenced differently by the deposit age and the bauxite origin. Taxonomical analysis revealed an early-stage microbial community dominated by haloalkaliphilic microorganisms and strongly influenced by chemical gradients. Microbial richness, diversity and network complexity increased significantly with the deposit age, reaching an equilibrium community composition similar to typical soils after decades of natural weathering. Our results suggested that salinity, pH, and toxic metals affected the bacterial community structure, while fungal community composition showed no clear correlations with chemical variations.

1. INTRODUCTION

Bauxite residue is a solid by-product generated during the production of alumina from bauxite. Alumina extraction is most often performed by the Bayer process, where bauxite is digested with large quantities of sodium hydroxide at temperatures between 150 and 250 °C (Evans, 2016). Depending on the process parameters and the origin of the bauxite, 0.7 to 2 tons of bauxite residues are produced per ton of alumina (International Aluminium Institute and European Aluminium, 2015). Over the last 10 years, the average annual production of alumina was 116 ± 15 Mt (World Aluminium, 2020), which corresponds to ~200 Mt of bauxite residue produced per year. In the absence of economically profitable large-scale applications, bauxite residues are commonly landfilled in large open-air deposit areas (BRDA), reaching a total of 4.5 Bt bauxite residue in storage at the present time (Dentoni et al., 2021).

Due to the physicochemical characteristics of bauxite residue i.e., high alkalinity, high salinity, high metal content and lack of nutrients, BRDAs pose a challenge to most living organisms (Di Carlo et al., 2020; Santini et al., 2015b) and represent a potential source of contamination for the surrounding terrestrial and aquatic ecosystems (Bouchoucha et al., 2019; Ren et al., 2018). Consequently, efforts have been made to remediate these deposits, usually by the addition of amendments (e.g. gypsum and organic matter) that attenuate their harsh conditions prior to the revegetation of the area (Bray et al., 2018; Khaitan et al., 2010). BRDAs have also been considered as a promising secondary source of valuable and critical metals, as these elements are concentrated by a factor of 2 in bauxite residues compared to the initial bauxite ore (Panda et al., 2021; Ujaczki et al., 2017; Vind et al., 2018). Critical metals are chemical elements characterized by their high economic relevance and supply risk (European Commission, 2020) and include metals crucial for information and energy technologies such as Co, Mg, Ba, V, Ge, Nb, Sr, Ga, platinoids (PGMs), and rare earth elements (REEs: Lanthanides (Ln), Y, Sc).

Recently, microbial-driven approaches have gained attention as viable and cost-effective methods for the management and valorization of urban and industrial wastes, including bauxite residue (Lyu et al., 2021; Panda et al., 2021; Santini et al., 2019). During in-situ remediation processes, native microbial communities have been shown to decrease the pH and salinity of the bauxite residue, as well as play an essential role in soil formation and plant growth (Di Carlo et al., 2019; Tian et al., 2020; Wu et al.,

2019). Microbial metal recovery strategies are also promising for the dissolution and recovery of elements of interest (e.g., Fe, Al, critical metals) from waste (Baniasadi et al., 2019; Dev et al., 2020; Maes et al., 2016). Out of all these techniques, bioleaching and microbial electrochemistry are among the most-studied methods (Dominguez-Benetton et al., 2018; Srichandan et al., 2019). In bauxite residues, these techniques are still at an early experimentation stage, although some promising results for REE recovery by bioleaching have been reported (Kiskira et al., 2021; Qu et al., 2019; Zhang et al., 2020).

More generally, microbial-driven strategies for waste management imply the use of microbial communities native to contaminated sites, which tend to thrive better in such harsh environments due to their unique metabolisms developed through natural selection (Ghosh et al., 2018; Ma et al., 2019; Roy et al., 2018; Sajjad et al., 2020). In addition, microbial communities are known to perform complex functions and are more robust to environmental fluctuations compared to pure cultures (Perez-Garcia et al., 2016; Wang et al., 2020; Zhang et al., 2008). Metagenomics studies based on Next Generation Sequencing have significantly expanded the identification and dynamics of microbial communities involved in different bioprocesses. However, the evolution of microbial communities in metal biorecovery experiments is still limited to a few weeks (Ma et al., 2017; Sajjad et al., 2020; Wang et al., 2020). Regarding bauxite residues, the identification of pioneer microbial communities and their dynamics during primary succession have been highlighted as research needs to improve microbial-driven bioremediation (Santini et al., 2015a). Nevertheless, to date, studies on microbial diversity in bauxite residue have focused on the responses of bacterial communities to remediation strategies, overlooking their active role in the process (Banning et al., 2011; Fourrier et al., 2020; Ke, 2021; Krishna et al., 2014; Schmalenberger, 2013; Wu et al., 2020).

This study aimed at exploring the microbial dynamics during primary succession in a BRDA from Southern France using an integrated physicochemical and biological approach. The specific objectives of this study were to (a) evaluate the effect of the deposit age and the ore origin on the geochemical characteristics of bauxite residue; (b) identify the first microbial communities colonizing BRDAs and their role in the establishment of new species; (c) determine the microbial community structure in the equilibrium stage of primary succession in BRDAs and the main geochemical factors
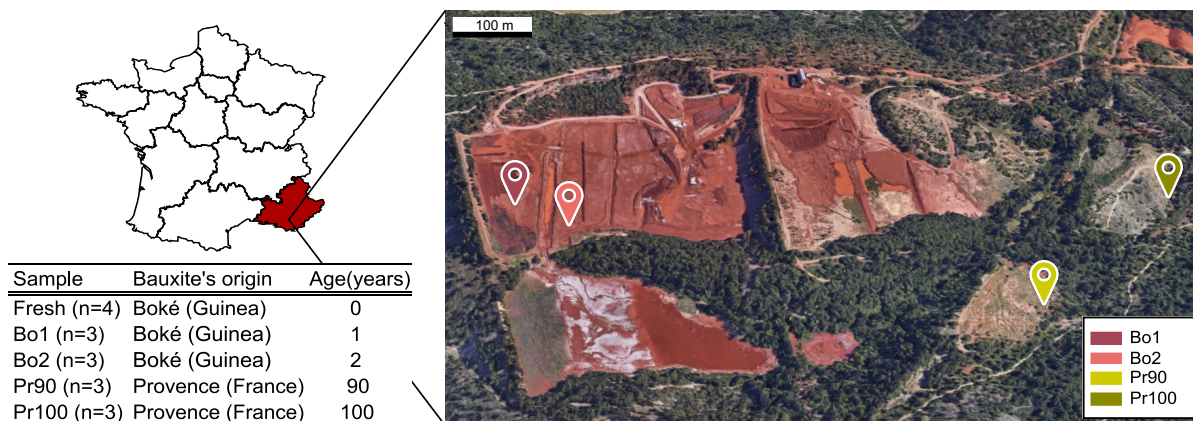
135 driving it; (d) explore possible implications of this study for microbial-driven
136 bioremediation and critical metal recovery.

137

138 **2. MATERIALS AND METHODS**

139 2.1 Site description and sampling

140 The bauxite residues come from a refinery operating the Bayer aluminum extraction
141 process since 1894 in Gardanne, Southern France. The sampling took place at the
142 Mange-Garri bauxite residue disposal area (BRDA) in Bouc-Bel-Air, Southern France.
143 This region is characterized by a hot-summer Mediterranean climate, with average
144 annual precipitation and temperature of 485 mm and 16.3°C (Copernicus Climate Data
145 Store, 2021). We selected four distinct areas of the BRDA based on their deposit age
146 (1, 2, 90, and 100 years) and bauxite origin (lateritic bauxite from Boké, Guinea (Bo)
147 and karstic bauxite from Provence, France (Pr)), named Bo1, Bo2, Pr90 and Pr100
148 (**Fig. 1**). At the Bo1 and Bo2 sites, bauxite residues were produced from Guinean
149 bauxite and were landfilled one and two years before sampling respectively. These
150 deposits are occasionally watered to prevent dust dispersion and were not amended
151 at the time of sampling. The Pr90 and Pr100 sites contain bauxite residues that were
152 produced from Provençal bauxite and were deposited around 90 and 100 years ago
153 respectively. These sites were amended with a soil layer in the 1960s and a slight
154 coverage with low-lying vegetation can be seen.

155 At each of the four sites, samples were collected in triplicate, gathering approximately
156 500 g of bauxite residue at a depth of 20 to 30 cm in sterile plastic bags. At sites Pr90
157 and Pr100, samples were collected at the edge of the deposit, where bauxite residues
158 were distant from the added soil layer. In addition, freshly produced bauxite residue (4
159 replicates) was also selected to analyze the initial bio-geochemical characteristics
160 before landfill. Samples were divided into two groups based on the following analyses.
161 Samples undergoing physicochemical analysis were oven-dried at 70°C, grounded in
162 a mortar, passed through a 130 μm sieve, and stored in metal-free plastic tubes.
163 Samples for microbial community analyses were stored at 4°C.

Sample	Bauxite's origin	Age(years)
Fresh (n=4)	Boké (Guinea)	0
Bo1 (n=3)	Boké (Guinea)	1
Bo2 (n=3)	Boké (Guinea)	2
Pr90 (n=3)	Provence (France)	90
Pr100 (n=3)	Provence (France)	100

Figure 1. Sampling site and samples description.

164

165   2.2 Physicochemical analyses

166   2.2.1 Elemental composition

167   First, pH and electrical conductivity (EC) were measured at a solid/MilliQ water ratio

168   of 1:5. Then, the elemental composition of the bauxite residues was determined after

169   alkaline fusion of the samples (Rivera et al., 2019). Briefly, 1 g of each sample was

170   digested with 750 mg of lithium tetraborate ($Li_2B_4O_7$) at 1000°C for 30 min (WiseTherm

171   F/FH 0-1200°C) and then immediately dissolved in 40 mL of HNO_3 1N. Prior to

172   elemental analysis, the samples were dissolved 200 times. Subsequently, inductively

173   coupled plasma mass spectrometry (ICP-MS, Perkin Elmer NexIon 300X) was used

174   to analyze elements with concentrations up to 1000 µg/L, while elements with

175   concentrations above 1000 µg/L were analyzed by inductively coupled plasma optical

176   emission spectroscopy (ICP-OES, Perkin Elmer 4300 DV). All analyses were

177   conducted for major and trace elements commonly found in bauxite residues, namely

178   Fe, Ti, Al, Ca, Zr, Cr, Mn, Zn, Th, Ni, Pb, Cu, Sn, Rb, Cs as well as critical raw elements

179   (as defined by the European Commission (2020): P, Mg, V, Lanthanides (Ln), Sr, Y,

180   Nb, Ba, Sc, Ga, Hf, Ge, Co, Sb, W, Ta). Total carbon (TC) and nitrogen were

181   determined by dry combustion using an Elemental Analyzer (Flash EA, Thermo

182   Scientific). To measure the total organic carbon (TOC), samples were treated with HCl

183   to remove carbonates before analysis.

184   2.2.2 Mineralogical composition

185   The mineralogical analyses of bauxite residue were carried out by X-ray diffraction

186   (XRD) using a PANalytical X'Pert Pro (Malvern Panalytical, UK) diffractometer

187   equipped with a cobalt tube (λ = 1.79 Å) running at 40kV and 40mA. Samples were

188 deposited on low background silicon plates and analyzed from 8° to 80° (2θ) with a
189 step size of 0.033° and a total counting time of 7 hours. Samples were also spun at
190 15 rpm to improve statistics. Phase identification was performed using the X'pert
191 Highscore plus software (PANalytical) together with the PDF-2 ICDD database
192 (International Center for Diffraction data, Powder Diffraction Files 2). Profex software
193 (Doebelin and Kleeberg, 2015) was used for Rietveld refinement to semi-quantify the
194 proportions of the minerals in the bauxite residues. The following parameters were
195 refined: zero point shift, sample displacement, cell parameters, preferred orientation
196 and peak broadening resulting from the size of the crystallite and the micro strain.

197 2.3 DNA extraction, PCR amplification and sequencing

198 The total DNA was extracted from 5 g of each bauxite residue samples using the
199 FastDNA® Spin Kit for soil (MP Biomedicals, USA) following the manufacturer's
200 protocol. Extracted DNA was used as template in separate PCR reactions amplifying
201 the bacterial 16S and the fungal ITS rRNA gene sequences. For bacterial diversity
202 analysis, we used the primers 341F (5'-CCTAYGGGRBGCASCAG-3') and 806R (5'-
203 GGACTACNNGGGTATCTAAT-3'), targeting the V3 and V4 variable regions of the
204 bacterial 16S rRNA (Caporaso et al., 2011; Muyzer et al., 1993). For fungal diversity
205 analysis, we used the primers fITS7 (5'-GTGARTCATCGAATCTTTG-3') and ITS4 (5'-
206 TCCTCCGCTTATTGATATGC-3'), targeting the ITS2 region (Ihrmark et al., 2012).
207 The amplification conditions were as follows: initial denaturation at 95 °C for 2 min;
208 followed by 34 cycles of denaturation at 95 °C for 30 s, annealing at 55 °C for 30 s,
209 and extension at 72 °C for 1 min; and a final extension at 72 °C for 5 min (Muller et
210 al., 2021). PCR products were then purified using ProNex® Size-Selective Purification
211 System (Promega, USA) and sequenced on Illumina MiSeq platform (Biofidal, Vaulx-
212 en-Velin, France). The raw sequence reads generated from this study have been
213 deposited in the National Center for Biotechnology Information (NCBI) Sequence
214 Read Archive under the accession number PRJNA748554.

215 2.4 Sequencing data processing

216 Microbiome bioinformatics were performed by the open-source software QIIME2,
217 version 2019.10 (https://qiime2.org) (Bolyen et al., 2019). Raw reads were quality-
218 filtered, denoised and chimera-checked using DADA2 (Callahan et al., 2016). DADA2
219 uses a parametric model to infer true biological sequences from reads. The model

220 relies on input read abundances (true reads are likely to be more abundant) and the
221 pairwise similarity between sequences. The taxonomic annotation of the resulting
222 sequence variants (ASVs) was assigned using the feature-classifier command with
223 default parameters in QIIME2 and sequences were matched against the Greengenes
224 13_8 database (McDonald et al., 2012). Finally, scaling with ranked subsampling
225 (SRS) curves (Beule and Karlovsky, 2020) were drawn to determine whether the
226 sequencing depth was sufficient to represent the true diversity of the samples.

227 2.5 Biodiversity parameters and microbial biomarker discovery

228 Alpha diversity was explored through observed ASVs, Chao1, and Shannon. The
229 observed ASVs and the Chao1 estimator were selected to identify community
230 richness, and Shannon index was used to assess community diversity (Callahan et
231 al., 2017; Hill et al., 2003). Beta diversity analysis was used to evaluate distribution
232 patterns in samples based on bacterial and fungal ASV composition (Anderson et al.,
233 2011; Callahan et al., 2017). For this purpose, a principal coordinate analysis (PCoA)
234 based on weighted UniFrac distances (Lozupone et al., 2007) was conducted. All
235 alpha and beta diversity metrics were calculated using QIIME 2 after normalization to
236 59388 and 4778 sequences per sample for bacteria and fungi, respectively. Linear
237 discriminant analysis effect sizes algorithm (LEfSe) (Segata et al., 2011) was
238 performed on the Galaxy platform (https://huttenhower.sph.harvard.edu/galaxy/) to
239 identify bacterial biomarkers characterizing the samples. LEfSe couples Kruskal–
240 Wallis tests for measuring statistical significance with quantitative tests for biological
241 consistency (Wilcoxon rank sum test).

242 2.6 Statistical analysis

243 All statistical analyses were performed with the open-source software R (R Core
244 Team, 2020) using the packages "dplyr" (Wickham et al., 2021), "vegan" (Oksanen et
245 al., 2020), "car" (Fox and Weisberg, 2019), "ggpubr" (Kassambara, 2020), and "rstatix"
246 (Kassambara, 2021). Figures were produced with the package "ggplot2" (Wickham,
247 2009). To study the ore-dependent differences in chemical and microbiological
248 compositions of bauxite residue, unpaired two-sided T-tests and Wilcoxon rank sum
249 tests were conducted respectively. Furthermore, Games-Howell post-hoc tests were
250 used to assess the age-dependent variations in chemical and microbial compositions.
251 Pearson correlations between each variable and the deposit age were used to further

252 explore these relationships. Also, significant differences in alpha diversity indices were
253 tested by Wilcoxon rank sum tests.

254 Principal component analysis (PCA) was used to identify the variables that explain
255 most of the variation in chemical composition. In addition, unsupervised hierarchical
256 clustering was applied to the PCA to group the samples according to their chemical
257 similarity. Both PCA and hierarchical clustering were performed using the packages
258 "FactoMineR" (Lê et al., 2008) and "factoextra" (Kassambara and Mundt, 2020).
259 PERMANOVA via the *adonis* function was conducted in both PCA and PCoA to test
260 for the chemical and microbiological dissimilarities based on the deposit age and the
261 bauxite origin. To study the factor age alone, nested PERMANOVA were calculated
262 using the parameter *strata* to exclude the effect of bauxite origin. Furthermore, multiple
263 co-inertia analysis (MCIA) was performed using the package "omicade4" (Meng et al.,
264 2014) to determine the relationships between the four datasets used in this study
265 (chemical characteristics, mineralogy, 16S rRNA sequences and ITS sequences).

266 2.7 Co-occurrence network construction

267 Co-occurrence analyses were implemented for a better understanding of bacterial and
268 fungal interactions in the four bauxite residues. Co-occurrence networks were
269 constructed based on pairwise Pearson correlations calculated between bacterial and
270 fungal ASVs by using the base R function *cor* (Berry and Widder, 2014; Williams et
271 al., 2014). To avoid including false positives in the network due to spurious or random
272 interactions, the ASV table we permuted 100 times and a *p*-value for each possible
273 pairwise interaction was calculated to test its validity. The *p*-values were then adjusted
274 using the Benjamini-Hochberg procedure (Benjamini and Hochberg, 1995), and only
275 edges with a *p*-value below 0.01 that corresponded to an absolute correlation higher
276 than 0.4 were retained. To describe the topology properties of the networks, a set of
277 network indexes including graph density, average degree of nodes, transitivity,
278 modularity, average geodesic distance, betweenness centrality, and density were
279 calculated with the R package "igraph" (Csardi and Nepusz, 2006). The Wilcoxon test
280 was employed to assess significant differences in topological parameters between
281 networks. The connectivity of the network nodes was determined by their within-
282 module connectivity (Z_i) and among-module connectivity (P_i). Nodes were then
283 classified into four categories, according to Poudel et al. (2016): peripherals ($Z_i < 2.5$
284 and $P_i < 0.62$, nodes with few links to other species), connectors ($P_i > 0.62$, nodes

285 that connect modules), module hubs ($Zi > 2.5$, highly connected nodes within
286 modules), and network hubs ($Zi > 2.5$ and $Pi > 0.62$, highly connected nodes among
287 and within modules).

288

289 **3. RESULTS**

290 **3.1.pH, EC and geochemical composition**

291 The pH of the bauxite residue ranged from 8.70 ± 0.34 to 11.90 ± 0.01, with the highest
292 value in fresh samples and the lowest in Pr100 (**Fig. 2a**, Table S1). The EC of the
293 bauxite residue ranged from 0.29 ± 0.15 mS/cm to 2.53 ± 0.04 mS/cm, and again,
294 fresh samples showed the highest value and Pr100 the lowest (**Fig. 2a**, Table S1).

295 The elements with the highest concentrations in all bauxite residue samples were Fe
296 (268894 ± 45706 mg/kg), Ti (51313 ± 17317 mg/kg), Al (33093 ± 5662 mg/kg), Ca
297 (22425 ± 4952 mg/kg), and TC (17162 ± 9439 mg/kg) (**Fig. 2b**, Table S2). Fe
298 represents at least 22 ± 3 % of the dried mass in all samples. The main critical
299 elements present in all samples were Ti (51313 ± 17317 mg/kg), P (2743 ± 1274
300 mg/kg), Mg (1877 ± 987 mg/kg), V (849 ± 423 mg/kg), Ln (775 ± 339 mg/kg), Sr (240
301 ± 142 mg/kg), Y (159 ± 59 mg/kg), Nb (99 ± 16 mg/kg), Sc (73 ± 12 mg/kg), Ba ($73 \pm$
302 15 mg/kg), and Ga (56 ± 24 mg/kg) (**Fig. 2c-d**, Table S2). TN concentrations were
303 only above the machine's limit of detection (100 mg/kg) in the Provence samples, with
304 values of 287 ± 183 mg/kg for Pr90 and 470 ± 158 mg/kg for Pr100 (Table S2).

305 Statistical analysis showed that Ti, Cr, V, and Ga concentrations were significantly
306 higher in samples coming from Boké bauxite ($p < 0.05$, Table S2), while samples from
307 Provence bauxite showed greater abundances of TC, TOC, P, Mg, Ln, Mn, Sr, Y, Sc,
308 Pb, Ni, and Co ($p < 0.05$, Table S2). Within these two groups, some elements
309 concentrations changed over time. In the Boké samples, a significant decrease in Fe,
310 Ca, Cr, V, Ga, Cu, Ge, and W was observed as sample age increased ($p < 0.05$, Table
311 S2) while Mg, and Sr concentrations increased with age ($p < 0.05$, Table S2). In the
312 Provence samples, Mg decreased significantly with age, while P and TOC
313 concentrations increased ($p < 0.05$, Table S2). These relationships between the age
314 of the sample and their chemical properties were further confirmed by Pearson
315 correlations ($R \geq 0.9$, $p < 0.05$, Fig. S1).
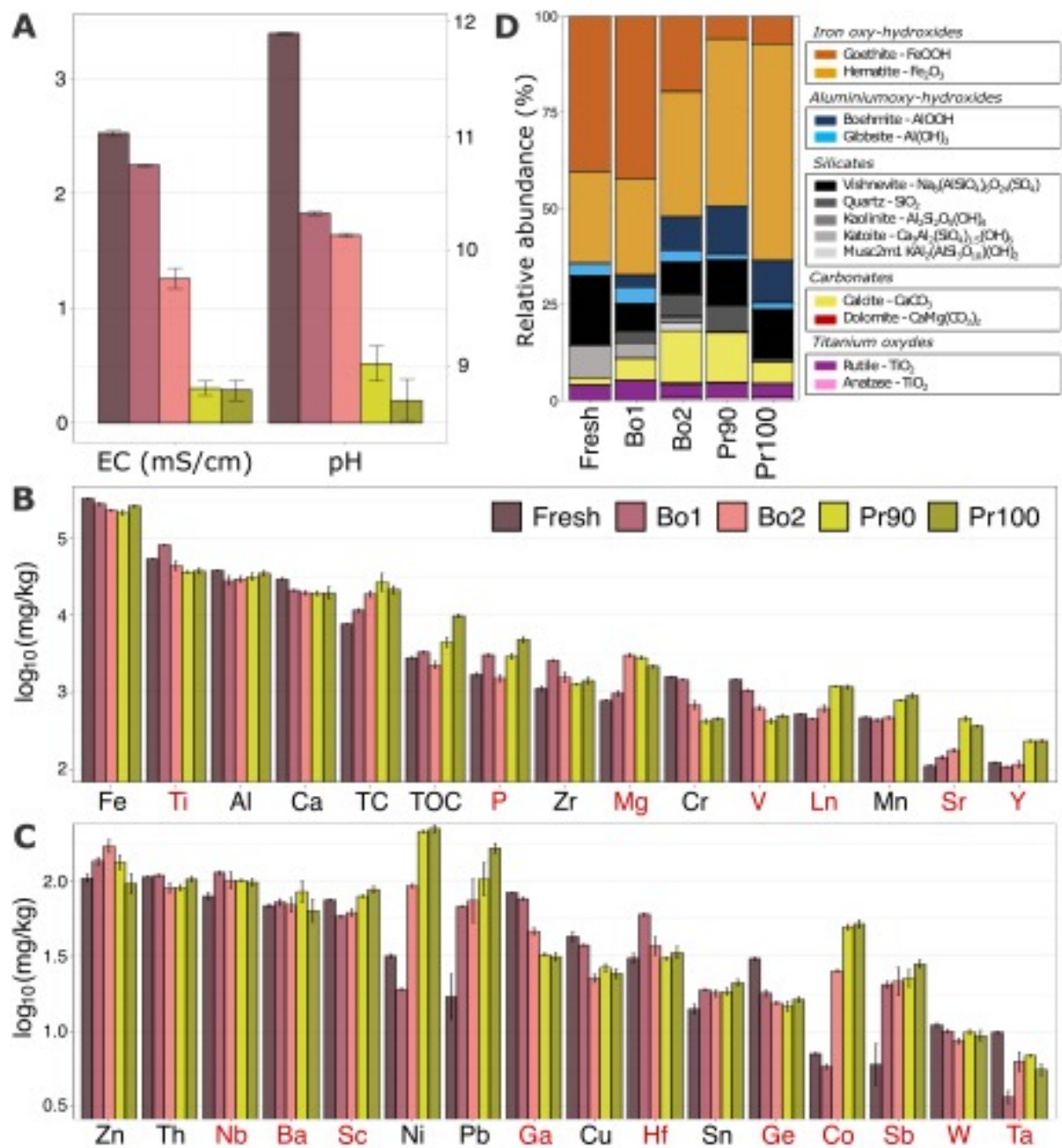
Figure 2. Physicochemical properties of bauxite residue samples. A) pH and EC, B) Major elements concentrations, C) Trace elements concentrations, and D) Mineralogy. Critical elements are colored red.

3.1.2 Element correlation

PCA was used to detect patterns in the chemical dataset and describe linear relations between the analyzed physicochemical parameters (**Fig. 3a**). The first three principal component axis (PC1, PC2, and PC3) explained 84.3% of the data variability between samples. PC1 explained 53.0% of the variance and included two groups: the first one

composed of pH, EC, Ga, Cr, V, Cu, Fe, Ge, Ca, Ti, and W whereas the second one comprised TOC, Co, Ni, Sr, Ln, Mg, Pb, Mn, Y, Sb, Cs, and Sn. PC2 explained 18.4% of the variance among samples and was mainly composed of Zr, Sc, Hf, Ta, Al, Zn, Nb, and Ti. Finally, PC3 (not shown) explained 12.9% of variance and was primarily composed of P, Th, Rb, Zn, Cs, and Sn. PERMANOVA analysis corroborated that the factors "age" ($p < 0.01$) and "bauxite origin" ($p < 0.05$) significantly explained the differences in chemical properties across samples. The factor "age" (tested by nested PERMANOVA to exclude the effect of the bauxite origin) explained 65.8% of the variance in chemical parameters while the factor "bauxite origin" explained 28.18%. The hierarchical cluster analysis (Fig. S2) provided statistical confirmation of the tendencies observed in the PCA and bauxite residue samples were clustered based on their chemical similarity. The first cluster contained the fresh samples, the second cluster Bo1 samples, the third cluster Bo2 samples, and the fourth cluster contained both Pr90 and Pr100 samples.

To further understand the effect of the factor "age" on residues generated from the same bauxite ore, a second PCA was conducted considering only the Boké samples (fresh, Bo1 and Bo2) (**Fig. 3b**). The first two dimensions explained 82.5% of the variability and the factor "age" separated the samples significantly (PERMANOVA, $p < 0.01$). Co, Sr, Pb, Mg, and Sb were mostly associated with Bo2, while pH, EC, W, Ca, Ge, Fe, Cu, V, Cr, and Ga had their highest values in fresh samples and decreased progressively with age. In contrast, TOC, Y, Mn, Ln, Ni, Sn, Al, and Ta did not show any age-dependent trends during the first years of storage (Table S2). Globaly, this statistical analysis is in line with the expected behavior of the elements, such as the colocalization of Cr and V and their correlation with Fe (Markus Gräfe et al., 2011) as well as the REEs affinity for Mn phases (Vind et al., 2018).
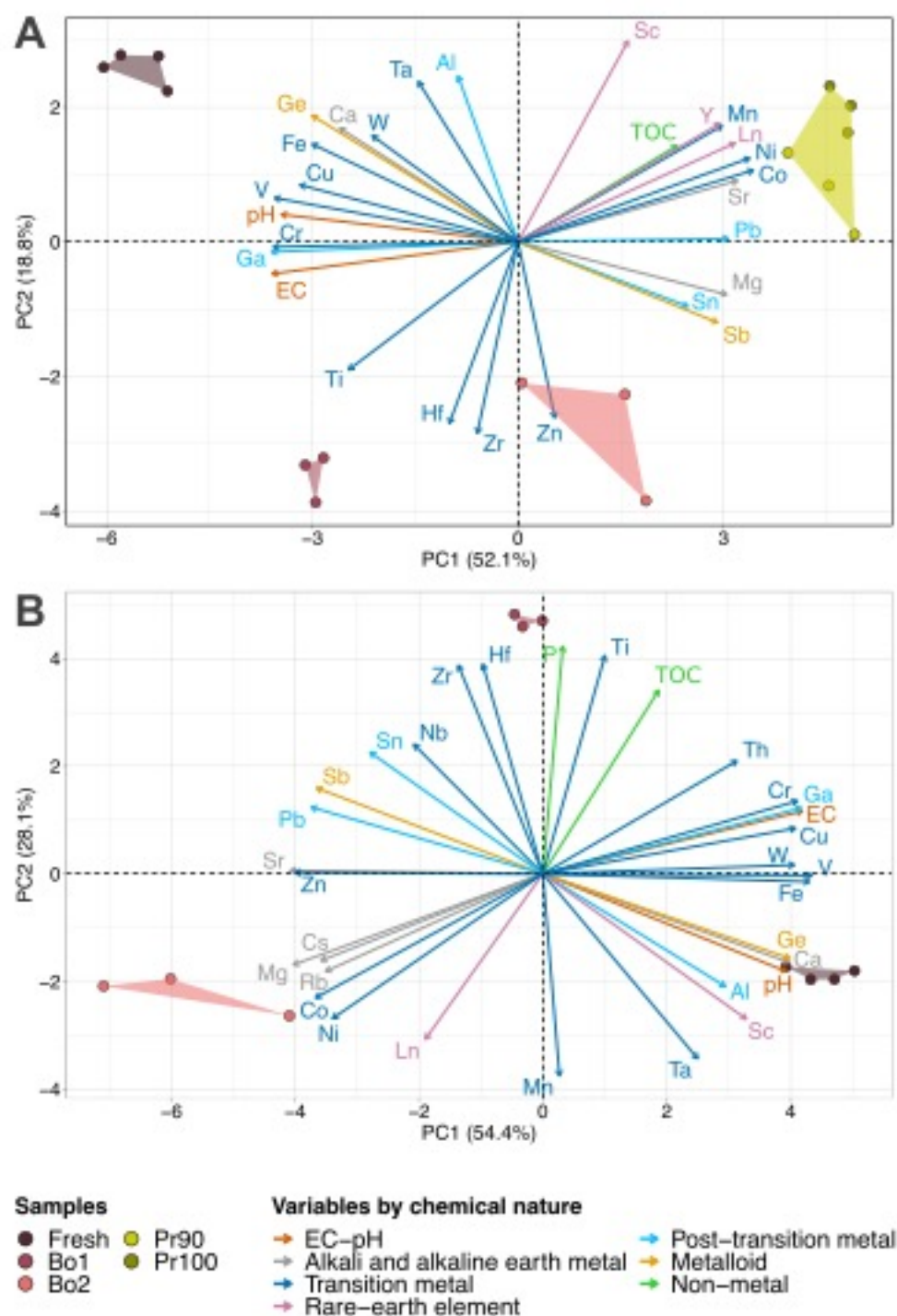
Figure 3. Principal component analysis (PCA) of chemical parameters in A) all and B) Boké bauxite residue samples. Individuals are represented by dots and colored by sample. Individuals are grouped according to hierarchical clustering results. Variables are represented by arrows and colored by chemical nature. Only variables with a $cos^2 > 0.5$ are shown.

347

348

3.1.3 Mineralogical composition

XRD analysis (**Fig. 2d**, Table S3) showed that bauxite residues were principally composed of iron and aluminum oxides, hydroxides, and silicates. Goethite (FeO(OH)), hematite (Fe_2O_3), gibbsite ($Al(OH)_3$), and vishnevite ($Na_8(AlSiO_4)_6O_{24}(SO_4)$) are the dominant phases and accounted for at least 70 % of the crystalline fraction in all the samples. Rutile (TiO_2) and calcite ($CaCO_3$) were also detected in all samples, in the range of 3-5 % and 2-14% respectively. The hematite, anatase (TiO_2) and boehmite (AlO(OH)) were significantly more present in Provence samples, and interestingly, neither anatase nor boehmite were found in fresh samples (Table S3). In Boké samples, a significant decrease in goethite and Katoite ($Ca_3Al_2(SiO_4)_{1.5}(OH)_6$) was observed as the age of the samples increased.

3.2 Microbial community diversity, structure and dynamics

3.2.1 Alpha diversity

The influence of bauxite residue's age and geochemical composition on microbial communities was assessed using 16S and ITS metabarcoding. As expected, no DNA could be extracted from the fresh residue samples. For Bo1, Bo2, Pr90, and Pr100, the sequencing achieved a coverage of more than 55000 16S rRNA sequences and 4700 ITS sequences per sample. The SRS curves (Fig. S3) indicated that the sequencing depth was sufficient to identify the majority of ASVs within bacterial and fungal communities in all the samples (except fresh samples). Alpha-diversity derived from the number of ASVs, Chao1 richness, and Shannon's index showed differences between samples regarding bacterial and fungal communities (Table S4). A total number of 7994 bacterial ASVs were identified, with 350 to 1318 ASVs per sample. The number of bacterial ASVs in the Provence samples (Pr90 and Pr100) was 6928, significantly greater than the 2867 ASVs found in the Boké samples (Bo1 and Bo2). The Provence samples also showed the highest richness and Shannon values for bacteria, compared with Boké samples (**Fig. 4a**). For fungi, 892 ASVs ranging from 45 to 156 ASVs per sample were obtained, with again more ASVs and Chao1 richness in Provence samples. However, there were no significant changes in Shannon's index between both group of samples, indicating that the specific diversity of the fungal communities was similar in Provence and Boké samples.
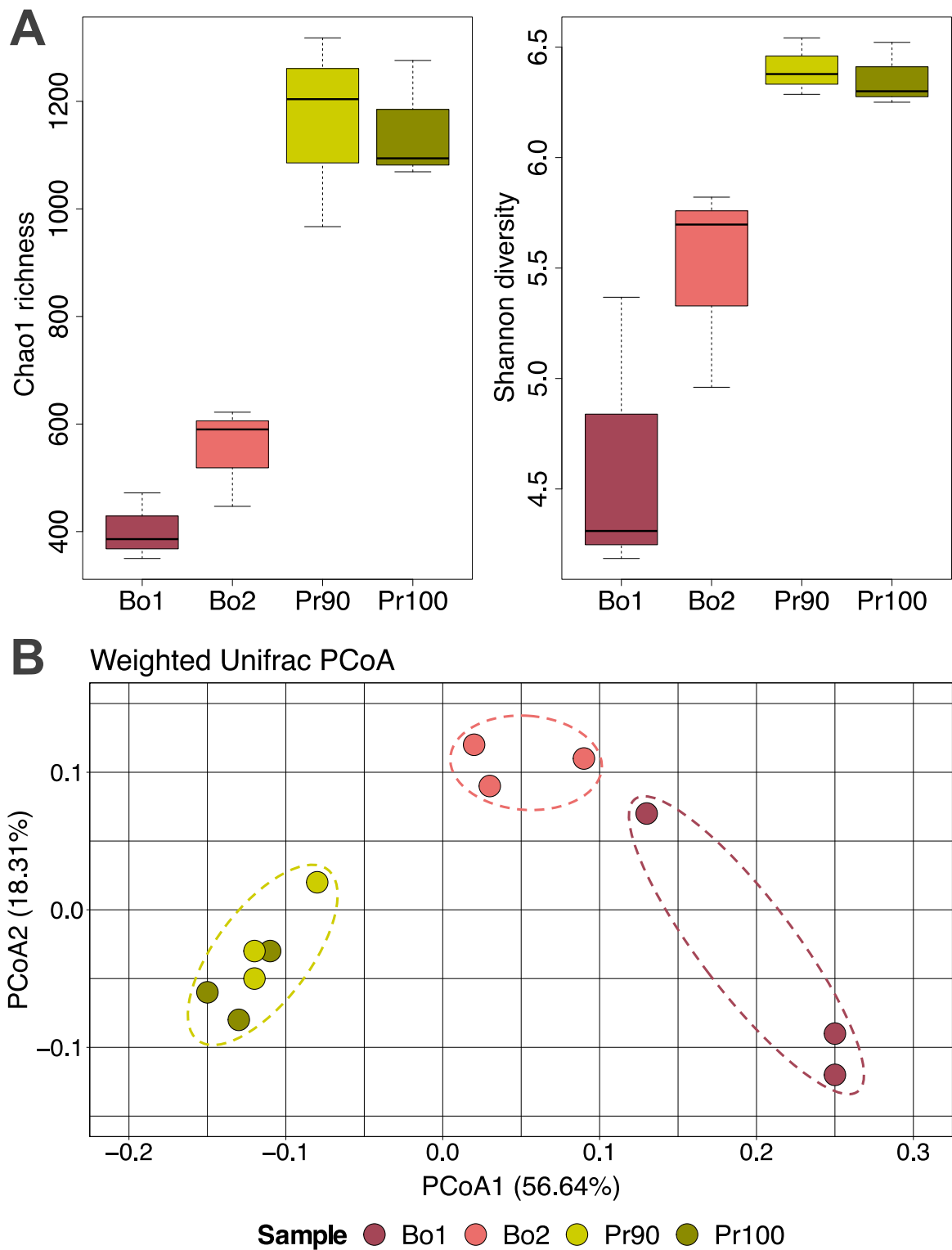
Figure 4. Bacterial alpha and beta diversity of bauxite residues. A) Chao1 richness and Shannon diversity index. B) Principal coordinate analysis (PCoA) based on weighted UniFrac distances between bauxite residue samples.

3.2.2 Microbial community structure

PCoA ordinations based on weighted UniFrac distances (**Fig. 4b**) revealed that the bacterial community structure differed between the bauxite residue samples. Samples were significantly separated based on bauxite origin (PERMANOVA, $p < 0.05$), and nested PERMANOVA confirmed the difference in bacterial community structure across age ($p < 0.001$). The first two axes of PCoA explained 74.95% of the community dissimilarity. Axis 1 was most correlated with EC ($R = 0.97$, $p = 1.1e-07$), followed by Co ($R = 0.96$, $p = 9.8e-07$), Ni ($R = 0.95$, $p = 1.4e-06$), Cr ($R = 0.94$, $p = 1.1e-07$), V ($R = 0.92$, $p = 2.5e-05$), Ti ($R = 0.9$, $p = 5.4e-05$), and pH ($R = 0.9$, $p = 8.1e-05$); while Axis 2 correlated with P ($R = 0.75$, $p = 0.005$). In contrast, the fungal community structure did not seem to follow a clear pattern among samples according to PCoA built on Bray-Curtis distances (Fig. S4).

The bacterial phyla that dominated all bauxite residue samples were Proteobacteria, Actinobacteria, Chloroflexi, Bacteroidetes, Gemmatimonaidetes, Planctomycetes, Verrucomicrobia, Acidobacteria and Firmicutes, accounting for more than 90% of the total bacterial communities (**Fig. 5**). When comparing the samples from Provence and Boké, significant taxonomic differences were observed. Actinobacteria and Gammaproteobacteria were the dominant taxa in the Boké samples with an average abundance of 28.0 % and 21.3 % respectively, followed by Chloroflexi (9.8 %) and Bacteroidetes (9.8 %). In the Provence samples, Actinobacteria (18.4 %) were still dominant while Gammaproteobacteria (4.8 %) and Bacteroidetes (3.6 %) lost prominence in favor of Alphaproteobacteria (12.0 %), Planctomycetes (9.6 %), Betaproteobacteria (6.3 %), and Deltaproteobacteria (3.2 %). Boké samples were significantly enriched in Actinobacteria, Gammaproteobacteria, Bacteroidetes and Firmicutes, whereas samples from Provence showed greater abundances of Alphaproteobacteria, Planctomycetes, Betaproteobacteria and Deltaproteobacteria ($p < 0.05$). Acidobacteria (10.3 %), barely found in Boké samples, showed a strong increase in Provence samples ($p < 0.05$). Chloroflexi, Gemmatimonaidetes and Verrucomicrobia were nearly constant across samples.
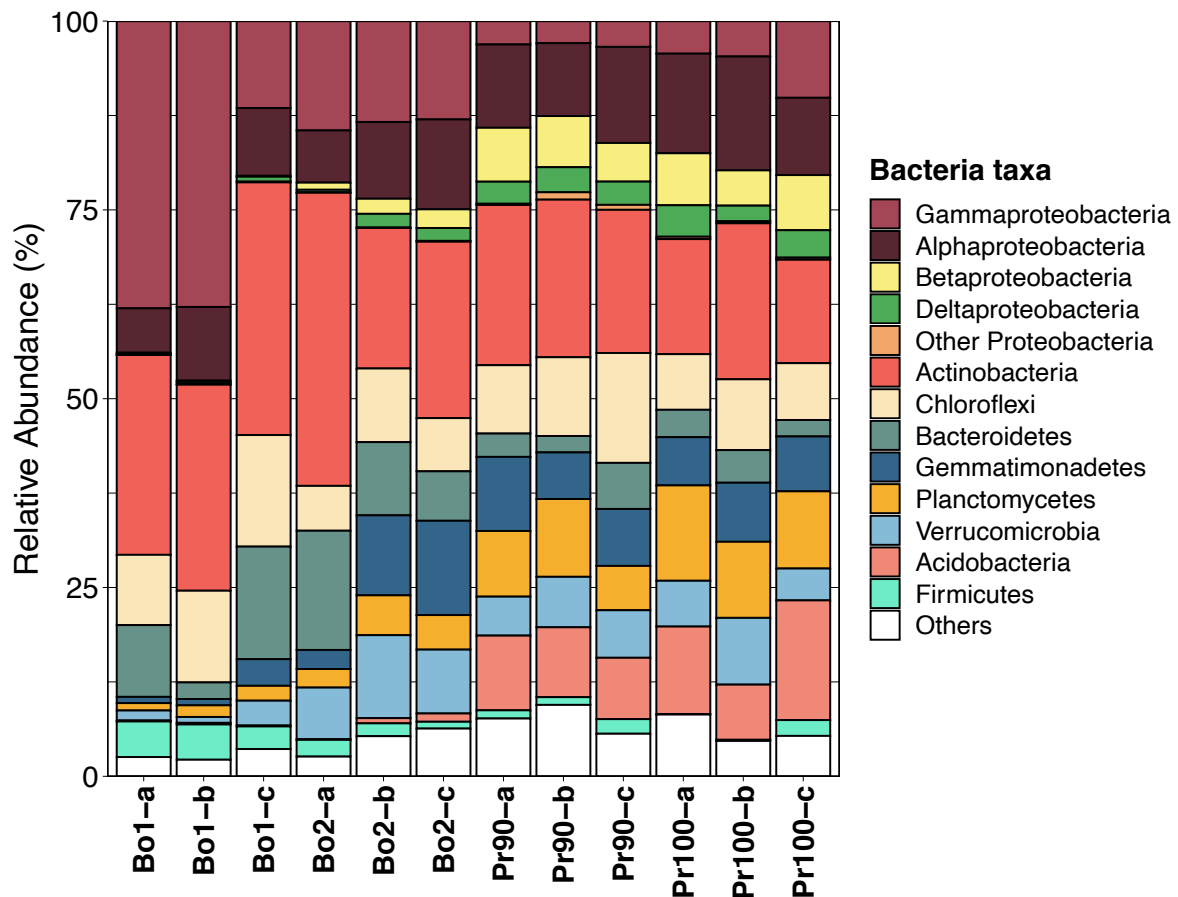
Figure 5. Relative abundance of the most abundant bacterial taxa among bauxite residue samples. Proteobacteria are divided in classes.

410

411 At the level of bacterial classes, differences between Boké and Provence samples
412 were also found (**Fig. 6**). Significantly higher proportions of Gammaproteobacteria,
413 Nitriliruptoria, Thermomicrobia, Gemm3, Bacilli, Rhodothermi, TK17, Deinococci and
414 Clostridia were identified in the Boké samples ($p < 0.05$). Within this group, variations
415 between samples of different ages were also observed. Bo1 was enriched in
416 Thermomicrobia, Thermoleophilia, Acidimicrobiia and Bacilli, whereas Opitutae,
417 Verrucomicrobiae and Flavobacteriia showed greater abundances in Bo2 ($p < 0.05$).
418 In contrast, Provence samples were significantly more enriched in
419 Alphaproteobacteria, Planctomycetia, Acidobacteria6, Betaproteobacteria,
420 Thermoleophilia, Deltaproteobacteria, Gemmatimonadetes, Pedosphaerae,
421 Anaerolineae, Phycisphaerae, Spartobacteria, Gemm1, Chloracidobacteria,
422 Ellin6529, S085, Nitrospira, Saprospirae, TK10, Solibacteres and TM71 ($p < 0.05$). In
423 the Provence samples, the only differences seen over ages were Pedosphaerae and
424 Actinobacteria, which were more abundant in Pr90 than in Pr100 ($p < 0.05$).
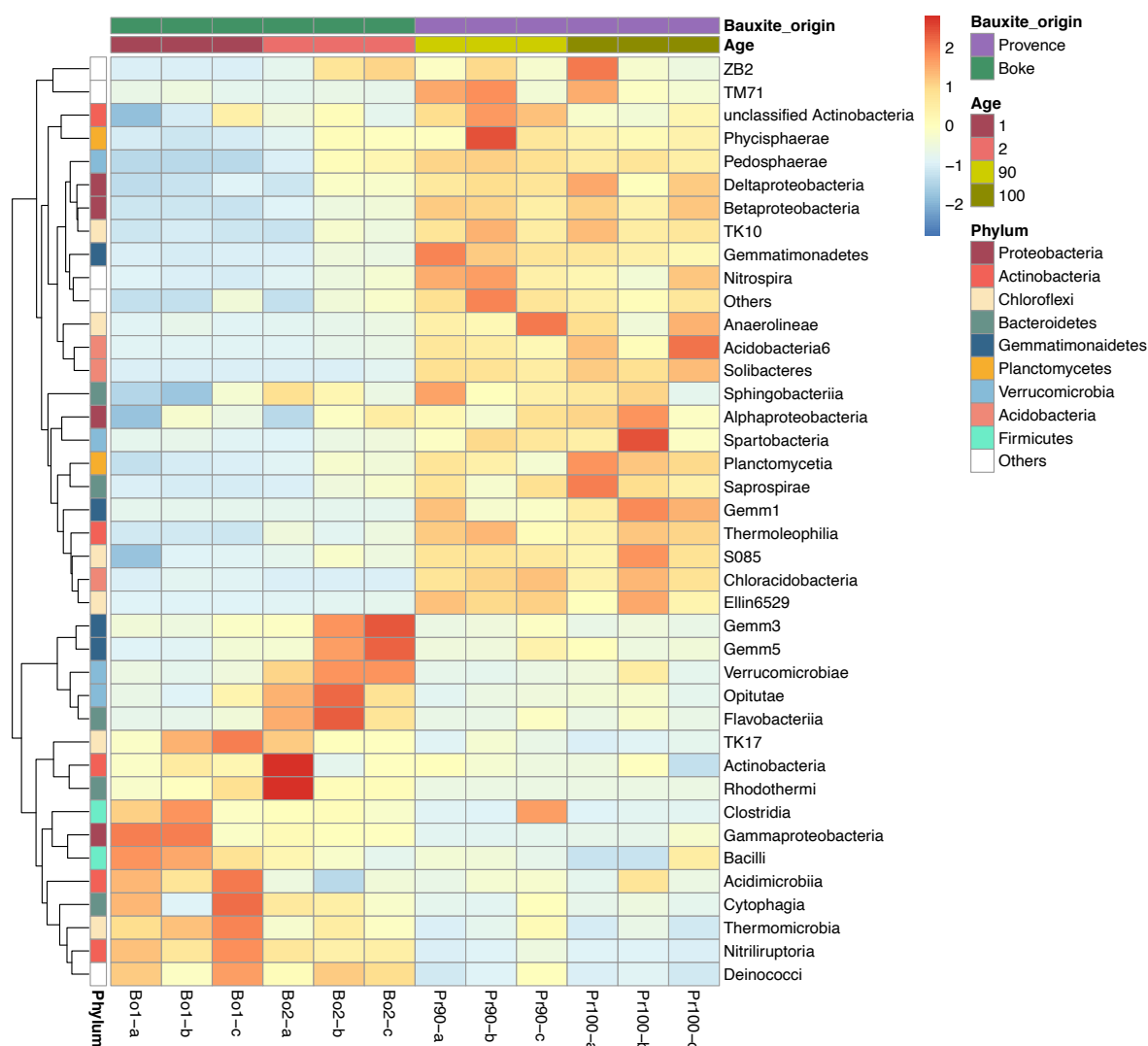
Figure 6. Z-score hierarchical clustering heat map representing the relative abundance of the top 40 bacterial classes in different bauxite residue samples.

425

3.2.3 Taxonomic characteristics of bacterial and fungal communities

426

To further explore these temporal scale differences, LEfSe analyses were conducted

427

to detect asymmetrically distributed bacterial taxa. Among the Boké samples, 9

428

indicator bacterial taxa were found in Bo1 against 37 in Bo2 (**Fig. 7a**). LEfSe confirmed

429

the highest abundance of three families of Bacilli in Bo1, as well as other taxa

430

belonging to the phyla Actinobacteria and Proteobacteria, and the archaeal class

431

Halobacteria. In line with our previous results, Opitutae, Verrucomicrobiae and

432

Flavobacteriia were significantly more abundant in Bo2, together with other taxa

433

belonging to the phyla Actinobacteria, Proteobacteria, Firmicutes, Bacteroidetes,

434

Planctomycetes and Nitrospirae. For the Provence samples, only two indicator

435

436   bacterial taxa (classified as Bacteroidetes) were identified in Pr90, against 28 in Pr100

437   (classified as Actinobacteria, Proteobacteria, Planctomycetes, Bacteroidetes,

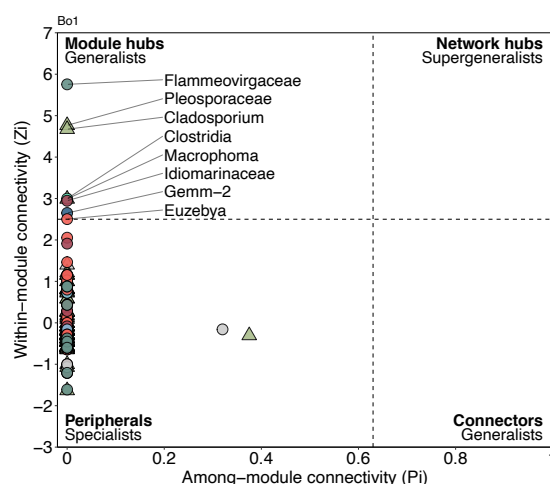438   Verrucomicrobia, and Chloroflexi) (**Fig. 7b**).
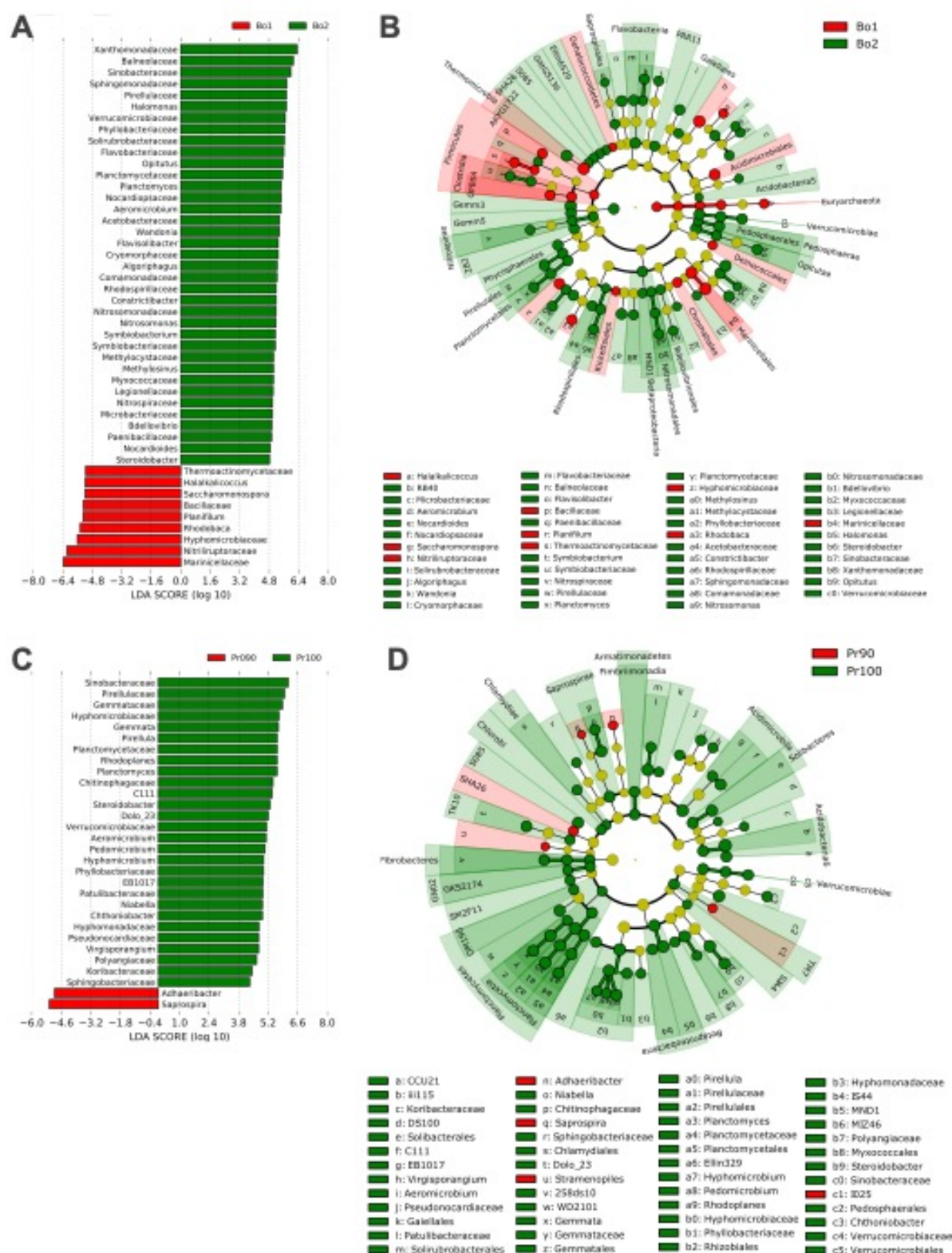
Figure 7. LEfSe analysis of in the bauxite residue samples according to sample age. Histograms of LDA scores of 16S gene sequences in Boké (A) and Provence (C) samples. Only taxa with a LDA score (log10) above 2.0 and a p-value lower than 0.05 for Kruskal–Wallis tests are shown. B and D Cladograms are derived from LEfSe analysis. The central point denotes the root of the tree and expanded to each ring representing the next lower taxonomic level from phylum to genus.

439

3.2.4 Microbial co-occurrence networks

440 Co-occurrence networks were constructed using the ASV data of 16S rRNA and ITS
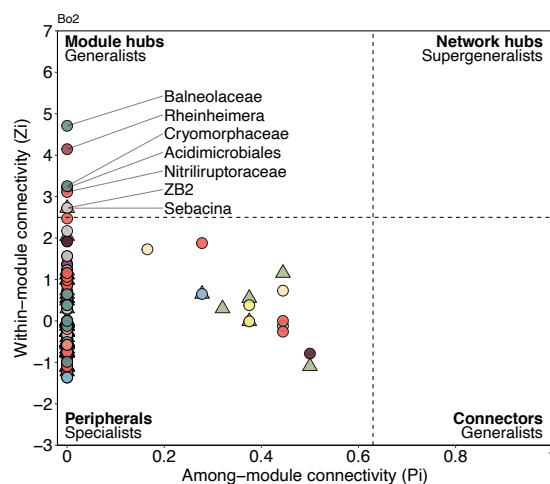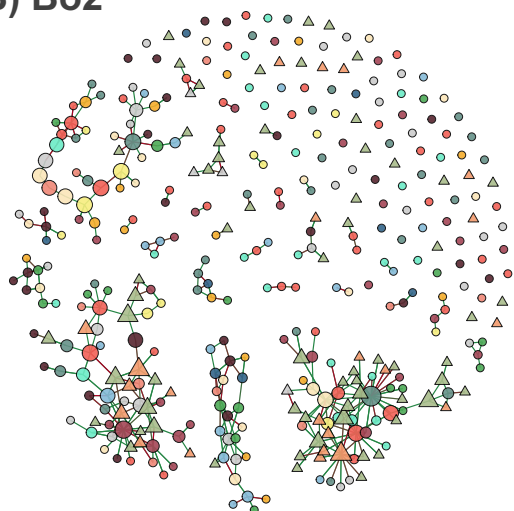
441 sequences. The Boké (**Fig. 8**) and Provence (**Fig. 9**) samples did not differ significantly

442 in network topological parameters such as average geodesic distance and modularity

443 (Table S5). However, the network complexity (number of nodes and edges, degree of

444 nodes, and transitivity) was different between the Boké and Provence networks (Table

445 S5). The two Boké networks (Bo1 and Bo2) contained a similar number of nodes (366

446 and 369), although Bo1 showed more edges (516 versus 324), higher average degree

447 (2.46 versus 1.76), and transitivity (0.15 versus 0.11). The two Provence networks

448 were more complex, as both Pr90 and Pr100 showed more nodes (603 and 571), more

449 edges (1254 and 1322), higher average degree (4.16 and 4.63), and higher transitivity

450 (0.18 and 0.12) compared to Boké.

451

452 Most of the nodes from the Boké and Provence networks were classified as

453 peripherals (specialists), and few nodes fell into module hubs (generalists) (**Fig. 8-9**).

454 Generalists are considered keystone taxa, as they are responsible for structuring the

455 different nodes and modules into a complete community, thus determining the

456 efficiency of energy metabolism and nutrient cycling in habitats (Wang et al., 2019). In

457 this study, more module hubs (generalists) were identified in Pr90 and Pr100 than in

458 Bo1 and Bo2. In Bo1 and Bo2 networks, the module hubs were mainly members of

459 Bacteroidetes, Actinobacteria, Proteobacteria, and Firmicutes for bacteria, and

460 Ascomycota for fungi. In contrast, the module hubs identified in Pr90 and Pr100

461 networks belonged to Proteobacteria, Actinobacteria, Chloroflexi, Verrucomicrobia,

462 Gemmatimonaidetes, Planctomycetes and Firmicutes for bacteria, and Ascomycota

463 and Basidiomycota for fungi.

Figure 8. Co-occurrence network and Zi-Pi plot of Bo1 (A) an Bo2 (B) bauxite residue samples. Each node represents a bacterial class (circles) or a fungal phyla (triangles). Nodes are colored by taxonomical affiliation and their size in the network is proportional to the node betweenness. The color of each link reflects positive (red) or negative (blue) interactions. The topological role of each node is defined by within-module connectivity (Zi) and among-module connectivity (Pi). According to values of Zi (2.5) and Pi (0.62), the roles of nodes are classified into four categories: Peripherals, Module hubs, Connectors and Network hubs.

464
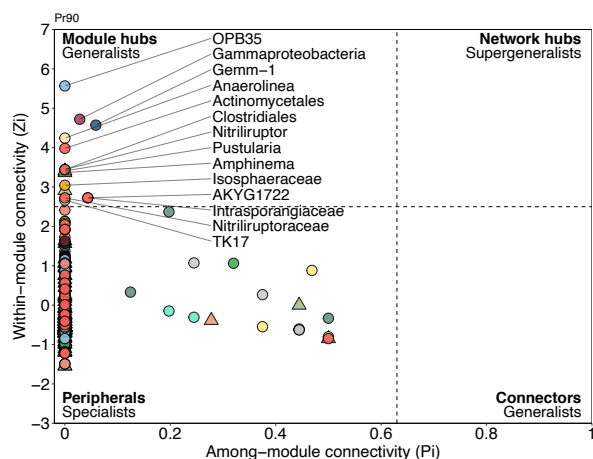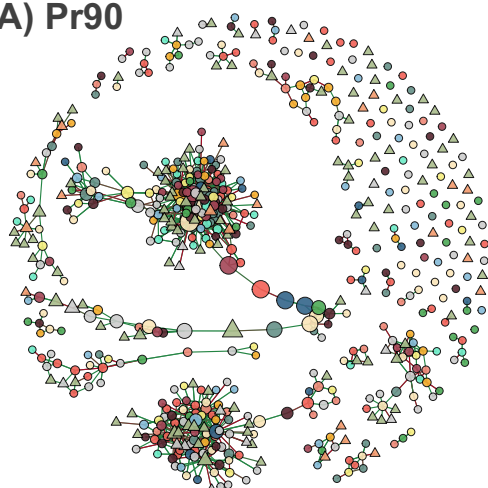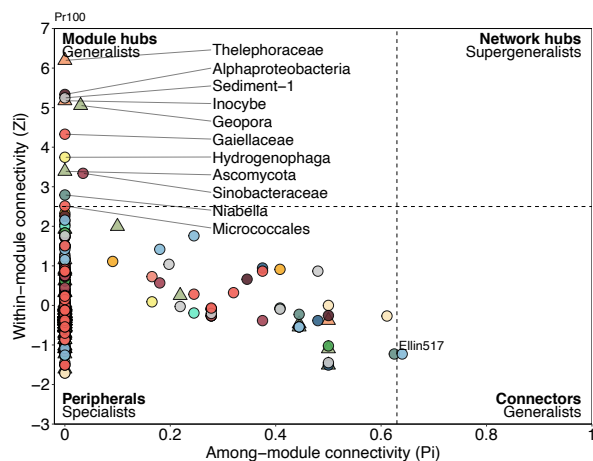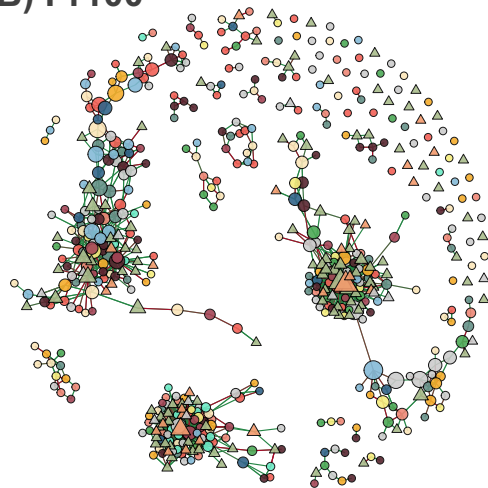
Figure 9. Co-occurrence network and Zi-Pi plot of Pr90 (A) an Pr100 (B) bauxite residue samples. Each node represents a bacterial class (circles) or a fungal phyla (triangles). Nodes are colored by taxonomical affiliation and their size in the network is proportional to the node betweenness. The color of each link reflects positive (red) or negative (blue) interactions. The topological role of each node is defined by within-module connectivity (Zi) and among-module connectivity (Pi). According to values of Zi (2.5) and Pi (0.62), the roles of nodes are classified into four categories: Peripherals, Module hubs, Connectors and Network hubs.

465

466

467

468

3.2.5 Multi co-inertia analysis

Multiple co-inertia analysis (MCIA) was used to determine the relationships between the chemistry, mineralogy, bacterial and fungal community composition in our bauxite residue samples. **Figure 10** displays the projection of the four datasets onto the first two principal components (PCs) of MCIA for Bo1, Bo2, Pr90 and Pr100 samples. PC1 and PC2 explained 54% and 19% of the total variation respectively (Fig. S6b). The sample space (Fig. S6a) shows a good correlation between the different datasets in all samples, which could be clearly differentiated. Early-stage bauxite residues (Bo1 and Bo2) were separated from equilibrium-stage samples (Pr90 and Pr100) along the PC1. Pseudo-eigenvalues (Fig. S6c) indicated that the chemistry and bacterial dataset contributed the most to the variation observed in PC1, while mineralogy was weighted in PC2. The pair-wise RV coefficient, which is multivariate generalization of the squared Pearson correlation coefficient, indicated higher global similarity between chemistry and bacterial classes (RV score = 0.86) when compared to the similarities between the chemistry and fungal classes (RV score = 0.36), and between the mineralogy and microbial classes (RV score for bacterial classes = 0.41, RV score for fungal classes = 0.22). Fungal classes contributed little to the variation of PC1 or PC2 and were mostly correlated with bacterial classes (RV score = 0.38).

Figure 10. MCIA analysis of bauxite residue samples. The figure shows the coordinates of the different data sets represented by shapes (circle: chemical data set; triangle: mineralogical data set; square: fungal classes data set; diamond: bacterial classes data set). Only bacterial and fungal classes representing at least 5% of the abundance in at least one sample are shown. Uncl. = unclassified; Alpha = Alphaproteobacteria; Gamma = Gammaproteobacteria.

4. DISCUSSION

4.1 BRDAs behave as primary successional environments

The initial geochemical conditions of the fresh bauxite residue, characterized by high alkalinity (pH = 11.90 ± 0.01) and salinity (EC = 2.53 ± 0.04 mS cm^{-1}) in line with previous studies (Cusack et al., 2019; Xue et al., 2016), make BRDAs hostile environments for most domains of life. The high pH and salinity derive from the excess of alkaline anions (hydroxides, carbonates, aluminates, aluminum hydroxides, silicates) and Na$^+$ produced during the Bayer process (Cusack et al., 2019; X. Kong et al., 2017) and thus the bauxite origin does not seem to significantly influence the value of these parameters. Fresh and recently deposited bauxite residues (Bo1 and

499   Bo2) also contained significant amounts of toxic metals for microorganisms, namely

500   Cr (1594 ± 23 mg/kg), V (1452 ± 10 mg/kg) and Al (38420 ± 920 mg/kg). The high

501   alkalinity (pH > 10) of fresh, Bo1 and Bo2 bauxite residues may favor the Cr (III)

502   oxidation to Cr(IV) as well as the predominance of V(V), both highly mobile and toxic

503   for bacteria, fungi and plants (Chen et al., 2021; Economou-Eliopoulos et al., 2016;

504   Liang et al., 2021; Milačič et al., 2012; Xiao et al., 2017). Regarding aluminum, only

505   1% of the total Al content in bauxite residue has been reported to be soluble at pH

506   values above 9, mainly as mobile $[Al(OH)^4]^-$ (Milačič et al., 2012). Nevertheless, its

507   impact on microbial and plant communities should not be neglected, as even small

508   proportions of the total Al correspond to potentially toxic concentrations. Moreover,

509   fresh and recently deposited bauxite residues were inherently poor in most

510   macronutrients required for microbial and plant growth, such as TOC, TN, and P

511   (Table S2). TOC accounted for less than 0.6% of the mass (0.28 % in fresh residue,

512   0.33 % in Bo1, and 0.23 % in Bo2) which is typically attributed to desert soils (Li et al.,

513   2013; Zech et al., 2014). TN concentrations were below the detection limit (100 mg/kg)

514   in fresh, Bo1 and Bo2 samples in agreement with previous studies (Krishna et al.,

515   2014; Wu et al., 2020). Finally, although the P concentrations ranged from 1500 to

516   3000 mg/kg in fresh, Bo1, and Bo2 samples, the available phosphorus in bauxite

517   residue is usually around 6.7 mg/kg (Santini et al., 2015a; Wu et al., 2020).

518   These extreme conditions, together with the absence of pre-existing life in the freshly

519   produced bauxite residues, indicate that BRDAs behave as primary successional

520   environments, similar to other well-studied natural systems (Guo et al., 2014; Schmidt

521   et al., 2008). Primary succession is characterized by an initial short phase where the

522   microbial community assembly is driven by stochastic dispersal processes, followed

523   by a longer deterministic phase dominated by environmental selection and competition

524   between species (Ortiz-Álvarez et al., 2018). In engineered environments like BRDAs,

525   the dispersal of microorganisms is limited, and environmental selection pressure is

526   usually stronger due to the extreme chemical characteristics of these sites. Therefore,

527   a shorter stochastic phase and a stronger deterministic assembly is expected in such

528   systems (Santini et al., 2015a). Given the environmental stress imposed by the

529   geochemical properties of fresh bauxite residues, the first pioneer microorganisms to

530   colonize BRDAs are likely to be haloalkaliphilic species able to accumulate nutrients

531 to facilitate the incorporation of new species (Santini et al., 2015a; Schmidt et al., 2014;
532 Sun et al., 2018).

4.2 Geochemistry-dependent microbial community assembly in the early stages
of primary succession

535 The bacterial community composition of the recently deposited bauxite residues (Bo1
536 and Bo2) was similar to that observed in soda lakes, alkaline residues, and other
537 unamended BRDAs (Bondici et al., 2013; Chakraborty et al., 2021; Kalwasińska et al.,
538 2017; Ohlsson et al., 2019), characterized by the dominance of Actinobacteria
539 (Actinobacteria, Nitriliruptoria, Acidimicrobiia) and Proteobacteria (especially
540 Gammaproteobacteria) and relatively high proportions (1 to 16 %) of Bacteroidetes
541 (Cytophagia, Rhodothermi, Flavobacteriia), Firmicutes (Bacilli, Clostridia), and other
542 alkalophilic classes (Opitutae, Deinococci) (**Fig. 5-6**).

543 The phyla Actinobacteria, Proteobacteria and Firmicutes contain some of the
544 prokaryotes best adapted to high alkalinity and salinity. Alkaliphilic and alkalinotolerant
545 microorganisms maintain their intracellular pH homeostasis by accumulating H^+ in
546 their cytoplasm trough Na^+/H^+ antiporters (Mamo, 2020). Our results showed that
547 Halobacteria (Archaea), Gammaproteobacteria, Nitriliruoptoria and Rhodothermi were
548 more abundant in Bo1 (**Fig. 6-7**) and correlated with EC (**Fig. 10**), corroborating the
549 preference of these classes for high-salinity niches (Zhang et al., 2019). Extreme
550 halophiles accumulate intracytoplasmic KCl to regulate their osmotic potential, which
551 constrains them to be obligate halophiles and limits their dispersal (Chen et al., 2020;
552 Shameer, 2016; Vaidya et al., 2018). Salinity (EC) decreased significantly from Bo1 to
553 Bo2 (**Fig. 1**, Table S2), allowing the proliferation of a wider range of halophilic and
554 halotolerant species such as Opitutae, Acidimicrobiia or the genus *Halomonas*
555 (Gammaproteobacteria) (**Fig. 6-7**). Halotolerant bacteria can flexibly adapt to habitats
556 with different salinities by synthesizing and accumulating compatible solutes in their
557 cytoplasm, which in turn requires a more intensive use of energy (Gunde-Cimerman
558 et al., 2018). Interestingly, the number of edges and network complexity was higher in
559 Bo1 compared with Bo2 (**Fig. 8**), indicating that saline stress promoted microbial
560 interaction as reported in other studies (Ji et al., 2019; Wang et al., 2019).

561 As pioneer colonizers, microorganisms are critical in the biogeochemical cycles and
562 the ensuing development of soil (Schmidt et al., 2008; Zeng et al., 2016). TOC

concentration showed no significant trend in early-stage samples (**Fig. 2**, Table S2), suggesting that the ratio in TOC input and consumption was balanced. In primary successional environments, the main sources of TOC are airborne allochthonous organic matter and C fixed by autotrophic microbial species (Ciccazzo et al., 2016). Our results also highlighted the significant abundance of heterotrophic bacteria in the early-stage samples, especially in Bo1, enriched in Actinobacteria and Bacteroidetes (**Fig. 6-7**). MCIA revealed that Cytophagia (Bacteroidetes) and Nitriliruptoria (Actinobacteria) correlated negatively with TOC (**Fig. 10**) and members of these classes were identified as keystone species in Bo1 (**Fig. 8**), confirming their relevance in oligotrophic habitats (Foreman et al., 2007; Gonzalez-Pimentel et al., 2018). Heterotrophic communities may represent the earliest stage of microbial assembly, degrading allochthonous organic compounds and supplying essential nutrients (TOC, N, P) for the subsequent development of autotrophic species (Hodkinson et al., 2002). Our results also indicated the presence of chemoautotrophic Proteobacteria typically involved in the primary production of alkaline environments (**Fig. 7**), including iron-oxidizing bacteria within Alphaproteobacteria (Rhodobacteraceae) and Betaproteobacteria (Comamonadaceae) (Jamieson et al., 2018; Kumaraswamy et al., 2006; Straub et al., 1996) and sulfur-oxidizing Chromatiales (Gammaproteobacteria) (Yuan et al., 2021). In tune with previous studies (Harantová et al., 2017; Schmidt et al., 2008), the abundance of non-symbiotic N-fixing bacteria, represented by members of Clostridia, Opitutae, Comamonadaceae (Betaproteobacteria), Rhodospirillales (Alphaproteobacteria) and Bacilli (Ciccazzo et al., 2016; Hingole and Pathak, 2013; Navarro-Noya et al., 2016), increased significantly after the first years of primary succession (**Fig. 5-6**). These bacteria could contribute to the slight increase in TN observed after the first years of bauxite residue weathering (Wu et al., 2020), undetectable in this study as it is expected to be less than 100 mg/kg. Nitrifying bacteria (Nitrosomonas and Nitrospiraceae) were also more prevalent in Bo2, confirming that, although the amount of ammonia derived from bacterial fixation is low at early stages of primary succession, it must be sufficient to fuel nitrification (Ollivier et al., 2011; Zeng et al., 2016). Moreover, our results suggest that the increase in N-cycle bacteria could be due to a significant decrease in EC and Cr in Bo2 (**Fig. 2**, **Fig. 10**, Table S2), as N-cycle enzymes are particularly sensitive to high salinity (Claros et al., 2010; Herbst, 1998) and heavy metal contamination (Kim et al., 2016; Oliveira and Pampulha, 2006).

4.3 Primary succession reaches an equilibrium in BRDA over few decades

The last stage of primary succession arises after long periods of time when the habitat becomes less harsh and environmental selection loses its strength in the assembly of communities, reaching an equilibrium (Ferrenberg et al., 2013). This maturity is expected to require more time to be developed in extreme geochemical systems as BRDAs. (Santini et al., 2015a). In our study, Pr90 and Pr100 samples, which have been naturally weathered for at least 90 years, did not show significant dissimilarities in either physicochemical parameters (**Fig. 3a**, Tables S1 and S2) or bacterial and fungal community composition (**Fig. 4b**; Fig. S5), suggesting that primary succession had reached the equilibrium in these sites. In Pr90 and Pr100, pH (8.8 ± 0.3) and salinity (EC = 0.29 ± 0.11 mS cm^{-1}) were significantly lower than in early-stage samples (**Fig. 2**, Table S1), revealing a significant dependence with the age of the samples. During bauxite residue natural weathering, salinity is generally assumed to decrease due to the dissolution of alkaline minerals by rainfall (Cusack et al., 2019; Zhu et al., 2016), while the decrease in pH is normally attributed to atmospheric and microbial carbonation (Cusack et al., 2019; Khaitan et al., 2010; Schmalenberger, 2013; X. Kong et al., 2017). Moreover, Pr90 and Pr100 showed a significantly higher concentration of macronutrients such as TOC, TN and P, which are accumulated during the bauxite residue natural aging due to the action of the different microorganisms that colonize the BRDAs (Santini et al., 2015a). This negative correlation between pH-salinity and age-nutrients is characteristic of restored and amended BRDAs (Courtney et al., 2014; Wu et al., 2021). Finally, our results also indicated a significant and steady decrease in Cr and V associated with the natural aging of the samples (**Fig. 2**, Table S2). However, the concentration of these metals also seems to be determined by the bauxite type and, therefore, the effect of the ore origin should not be neglected (Gentzmann et al., 2021).

Both alpha and beta bacterial diversity increased significantly in the equilibrium-stage samples (**Fig. 4**), in line with the results observed in restored BRDAs (Krishna et al., 2014; Wu et al., 2021, 2020). Beta-diversity analysis confirmed that "age" was the main factor explaining the dissimilarities of microbial community between Bo1/Bo2 and Pr90/Pr100 and not the ore origin. In addition, the changes in beta-diversity could be explained by pH, EC and some metal concentration gradients, all of them strongly anti-correlated with the age of the samples (**Fig. 3**). Circumneutral pH, lower salinity and

metal concentration, and increase in macronutrients support the survival of a more diverse microbial community dominated by bacteria commonly found in ordinary soils and freshwater like Alphaproteobacteria, Betaproteobacteria, Planctomycetes, Gemmatimonaidetes, and Acidobacteria. Acidobacteria are one of the most abundant terrestrial bacterial taxa, reaching 52% from the total bacterial community in certain soils (Kielak et al., 2016). Their abundance is positively correlated with low pH (Jones et al., 2009), and their accumulation over time in BRDAs is commonly associated with the restoration of chemical conditions in bauxite residue (Santini et al., 2015b; Wu et al., 2021). The equilibrium-stage bauxite residue also harbors a more complex microbial network, accounting for more highly connected taxa (nodes) than early-stage residues. Nutrient availability and higher microbial richness have been shown to favor microbial network complexity and the emergence of new ecological functions, making the ecosystem more stable (Qiu et al., 2021; Wagg et al., 2019).

In contrast, fungal biodiversity and community structure did not appear to be significantly affected by chemical gradients (Table S4, Fig. S5). The fungal community structure in early-stage bauxite residues was dominated by Ascomycota (80.1 ± 9.8 % of fungal communities), and Basidiomycota (> 14 %). This distribution seems to be the usual in natural and engineered haloalkaline environments, although the analysis of fungal communities in these habitats is limited to few studies (Grum-Grzhimaylo et al., 2016; Salano et al., 2017; Santini et al., 2015b). In the equilibrium-stage samples, the relative abundance of Ascomycota decreased (52.1 ± 24.2 %) while Basidiomycota (mostly Agaricomycetes) increased (35.0 ± 23.3 %). This pattern has been observed in restored BRDAs and was attributed to a decrease in total alkalinity (Santini et al., 2015b). In this study however, MCIA revealed a poor correlation between fungal communities and chemical parameters (RV score = 0.36). It is known that the fungal community assembly is more influenced by stochastic processes in primary successional environments (Schmidt et al., 2014). Unlike bacteria, climate is often considered the main environmental factor affecting the fungal community composition, rather than soil chemical properties (Egidi et al., 2019). Interestingly, all fungal keystones identified in Bo1 (**Fig. 8**) belonged to the class Dothideomycetes (Pleosporaceae, Macrophoma, Cladosporium), within the Ascomycota. Dothideomycetes constitute almost the entire fungal community in microbial mats from soda lakes and are also found in microbial mats from hypersaline and iron-rich habitats

663   (Gerea et al., 2012; Maza-Márquez et al., 2021; Salano et al., 2017). In microbial mats,
664   fungi play a crucial role in nutrient recycling by decomposing complex carbohydrates
665   into simpler compounds that fuel chemoheterotrophic species (Carreira et al., 2020).

4.4 Implications for bioremediation and metal recovery

667   To date, only few studies have focused their efforts on an integrated chemical,
668   physical, and biological approach for the characterization of BRDA in the optic of
669   bioremediation or critical metal bio extraction strategies.

670   Our results highlight the key role of pH and EC for natural microbial restoration and
671   therefore should be considered primary targets in bioremediation. If natural weathering
672   appears to be effective in reducing both pH and EC, it is also a slow process that could
673   be artificially accelerated. In the last few years, microbially-driven pH neutralization
674   using organic acids and CO_2 produced by fermentation of added carbon sources has
675   gained attention as a promising technique for in-situ bioremediation of BRDAs (Santini
676   et al., 2021; Wu et al., 2019). Santini et al. (2021, 2016) proved that the efficiency of
677   this process could be improved by decreasing the initial pH and salinity and increasing
678   the biodiversity of the microbial inoculum. However, they also identified the shortage
679   of nutrients (N and P) in the medium term as a limiting factor for the development of
680   this methodology. Our results suggest that lowering EC increased biodiversity and
681   facilitated the development of bacteria related to the N cycle. Hence, a first treatment
682   focused on reducing salinity (and pH if possible) before bacteria-mediated pH
683   neutralization could yield considerably better results. Few studies have investigated
684   the effect of lowering artificially pH and EC in the optic of bioremediation of BRDAs
685   (Courtney et al., 2014; Jones et al., 2011; Wong and Ho, 1994). As a recent example,
686   the recent study by Fourrier et al. (2021) has reported the positive effect of gypsum
687   addition and repeated washing on pH neutralization and EC decrease. In addition,
688   fungal contribution to early-stage microbial assembly seems to be underrated and their
689   role in bauxite residue remediation needs more research. Regarding microbially-
690   driven strategies for metal bio-extraction, our study is particularly informative for
691   selecting appropriate bauxite residue and bacteria for the selective extraction of critical
692   metals. In agreement with literature (Rivera et al., 2019; Vind et al., 2018), our results
693   indicated that the concentration of REEs (Ln, Sc and Y) in bauxite residue is primarily
694   determined by the ore origin, with karst bauxite (Pr90 and Pr100) being more enriched
695   in REEs than laterite bauxite (Fresh, Bo1 and Bo2). In addition, Y and Ln were strongly

correlated as expected regarding the analogy between Y and heavy REEs while Sc behaves differently to Y and Ln and is likely incorporated in iron oxyhydroxyde such as goethite (Levard et al., 2018). The conventional methods to recover these metals are not environmentally acceptable due to their excessive energy consumption and the production of hazardous residues, that require further treatment and high operating costs (Baniasadi et al., 2019). Metal bio-extraction is an interesting alternative to traditional mettalurgy that has still been poorly investigated for critical metals. Among the ideas that could benefit from our study, alkaline-active exoenzymes produced by bacteria found in Bo1 and Bo2 offer interesting possibilities for the valorization of bauxite residue. Despite their ability to lower their intracellular pH and salinity, haloalkaliphilic species must still be able to secrete stable and operational enzymes at elevated pH and salinity (Mamo, 2020), making BRDAs potential sources of these enzymes. Some of the haloalkaliphilic bacteria known to synthesize alkaline-active enzymes, namely Gammaproteobacteria, Actinobacteria and Firmicutes (Kalwasińska et al., 2018; Litchfield, 2011; Maharaja et al., 2018; Shameer, 2016; Shivlata and Tulasi, 2015), are also capable to modify the chemical phase and mobility of various critical metals (Chidambaram et al., 2010; Presentato et al., 2020; Wee et al., 2014), including REEs. For example, Maleke et al. (2019) reported the direct reduction of Eu^{3+} to Eu^{2+} by *Clostridium* sp. (Firmicutes). In line with previous studies (Santini et al., 2015b), the majority of Gammaproteobacteria corresponded to uncharacterized lineages, highlighting the potential of this group as a phylogenetic hot spot for novel haloalkaliphilic taxa.

5. CONCLUSIONS

In summary, this paper presents an integrated physicochemical and biological approach to explore the composition and dynamics of bacterial and fungal communities in bauxite residues deposited at different times and produced from different bauxite ores. Our results revealed that both deposit age and ore origin affect the geochemistry of bauxite residue, although unequally. Salinity, pH, TOC, TN, and P values seem to depend predominantly on the natural aging of bauxite residue, while the content of REE is mainly influenced by the origin of the bauxite ore. Our results highlight the behavior of bauxite residue deposits as primary successional environments and bring new insights into the early stages of microbial community

assembly in these sites. The pioneer microbial community was dominated by haloalkaliphilic microorganisms, strongly influenced by chemical gradients. Autotrophic and heterotrophic microbial species contribute to the supply of nutrients necessary for the development of other species through C fixation and degradation of allochthonous organic compounds, respectively. After the first years of natural restoration, nitrogen-fixing bacteria increase their presence and contribute to enhance N bioavailability. Microbial richness, diversity and network complexity increased significantly with age of deposition, until primary succession equilibrium was reached decades later, characterized by a microbial community composition similar to that of typical soils and freshwater. Our results suggested that salinity, pH, nutrients, and toxic metals (mainly Cr and V) were the main factors explaining this change in microbial communities. These results confirm the key role of pH and salinity in the establishment of early microbial communities and highlight them as main targets for bioremediation. Moreover, our co-occurrence network data suggest an important role of fungal communities in structuring the early-stage microbial community during primary succession, potentially by recycling complex organic matter. We also identified bacteria with potential metal extraction abilities, such as secretion of alkaline-active enzymes that could modify the chemical phase of the metals present.

Author contributions: Conceptualization C.L., W.A., M.A.; Data curation L.A.M-P.; Formal analysis L.A.M-P.; Funding acquisition C.L., W.A., M.A.; Investigation L.A.M-P.; Methodology L.A.M-P., B.A., D.B., M.B., L.P.; Project administration C.L., W.A., M.A.; Supervision C.L., W.A., M.A.; Validation C.L., W.A., M.A., L.A.M-P., B.A., D.B. M.B., L.P.; Writing - original draft L.A.M-P.; Writing - review & editing L.A.M-P., C.L., W.A., M.A. All authors have read and agreed to the published version of the manuscript.

6. REFERENCES

Anderson, M.J., Crist, T.O., Chase, J.M., Vellend, M., Inouye, B.D., Freestone, A.L., Sanders, N.J., Cornell, H.V., Comita, L.S., Davies, K.F., Harrison, S.P., Kraft, N.J.B., Stegen, J.C., Swenson, N.G., 2011. Navigating the multiple meanings of β diversity: a roadmap for the practicing ecologist. Ecol. Lett. 14, 19–28. https://doi.org/10.1111/j.1461-0248.2010.01552.x

Baniasadi, M., Vakilchap, F., Bahaloo-Horeh, N., Mousavi, S.M., Farnaud, S., 2019. Advances in bioleaching as a sustainable method for metal recovery from e-waste: A review. J. Ind. Eng. Chem. 76, 75–90. https://doi.org/10.1016/j.jiec.2019.03.047

Banning, N.C., Phillips, I.R., Jones, D.L., Murphy, D.V., 2011. Development of Microbial Diversity and Functional Potential in Bauxite Residue Sand under Rehabilitation. Restor. Ecol. 19, 78–87. https://doi.org/10.1111/j.1526-100X.2009.00637.x

Benjamini, Y., Hochberg, Y., 1995. Controlling the False Discovery Rate: A Practical and Powerful Approach to Multiple Testing. J. R. Stat. Soc. Ser. B Methodol. 57, 289–300. https://doi.org/10.1111/j.2517-6161.1995.tb02031.x

Berry, D., Widder, S., 2014. Deciphering microbial interactions and detecting keystone species with co-occurrence networks. Front. Microbiol. 5, 219. https://doi.org/10.3389/fmicb.2014.00219

Beule, L., Karlovsky, P., 2020. Improved normalization of species count data in ecology by scaling with ranked subsampling (SRS): application to microbial communities. PeerJ 8, e9593. https://doi.org/10.7717/peerj.9593

Bolyen, E., Rideout, J.R., Dillon, M.R., Bokulich, N.A., Abnet, C.C., Al-Ghalith, G.A., Alexander, H., Alm, E.J., Arumugam, M., Asnicar, F., Bai, Y., Bisanz, J.E., Bittinger, K., Brejnrod, A., Brislawn, C.J., Brown, C.T., Callahan, B.J., Caraballo-Rodríguez, A.M., Chase, J., Cope, E.K., Da Silva, R., Diener, C., Dorrestein, P.C., Douglas, G.M., Durall, D.M., Duvallet, C., Edwardson, C.F., Ernst, M., Estaki, M., Fouquier, J., Gauglitz, J.M., Gibbons, S.M., Gibson, D.L., Gonzalez, A., Gorlick, K., Guo, J., Hillmann, B., Holmes, S., Holste, H., Huttenhower, C., Huttley, G.A., Janssen, S., Jarmusch, A.K., Jiang, L., Kaehler, B.D., Kang, K.B., Keefe, C.R., Keim, P., Kelley, S.T., Knights, D., Koester, I., Kosciolek, T., Kreps, J., Langille, M.G.I., Lee, J., Ley, R., Liu, Y.-X., Loftfield, E., Lozupone, C., Maher, M., Marotz, C., Martin, B.D., McDonald, D., McIver, L.J., Melnik, A.V., Metcalf, J.L., Morgan, S.C., Morton, J.T., Naimey, A.T., Navas-Molina, J.A., Nothias, L.F., Orchanian, S.B., Pearson, T.,

Peoples, S.L., Petras, D., Preuss, M.L., Pruesse, E., Rasmussen, L.B., Rivers, A., Robeson, M.S., Rosenthal, P., Segata, N., Shaffer, M., Shiffer, A., Sinha, R., Song, S.J., Spear, J.R., Swafford, A.D., Thompson, L.R., Torres, P.J., Trinh, P., Tripathi, A., Turnbaugh, P.J., Ul-Hasan, S., van der Hooft, J.J.J., Vargas, F., Vázquez-Baeza, Y., Vogtmann, E., von Hippel, M., Walters, W., Wan, Y., Wang, M., Warren, J., Weber, K.C., Williamson, C.H.D., Willis, A.D., Xu, Z.Z., Zaneveld, J.R., Zhang, Y., Zhu, Q., Knight, R., Caporaso, J.G., 2019. Reproducible, interactive, scalable and extensible microbiome data science using QIIME 2. Nat. Biotechnol. 37, 852–857. https://doi.org/10.1038/s41587-019-0209-9

Bondici, V.F., Lawrence, J.R., Khan, N.H., Hill, J.E., Yergeau, E., Wolfaardt, G.M., Warner, J., Korber, D.R., 2013. Microbial communities in low permeability, high pH uranium mine tailings: characterization and potential effects. J. Appl. Microbiol. 114, 1671–1686. https://doi.org/10.1111/jam.12180

Bouchoucha, M., Chekri, R., Leufroy, A., Jitaru, P., Millour, S., Marchond, N., Chafey, C., Testu, C., Zinck, J., Cresson, P., Mirallès, F., Mahe, A., Arnich, N., Sanaa, M., Bemrah, N., Guérin, T., 2019. Trace element contamination in fish impacted by bauxite red mud disposal in the Cassidaigne canyon (NW French Mediterranean). Sci. Total Environ. 690, 16–26. https://doi.org/10.1016/j.scitotenv.2019.06.474

Bray, A.W., Stewart, D.I., Courtney, R., Rout, S.P., Humphreys, P.N., Mayes, W.M., Burke, I.T., 2018. Sustained Bauxite Residue Rehabilitation with Gypsum and Organic Matter 16 years after Initial Treatment. Environ. Sci. Technol. 52, 152–161. https://doi.org/10.1021/acs.est.7b03568

Callahan, B.J., McMurdie, P.J., Holmes, S.P., 2017. Exact sequence variants should replace operational taxonomic units in marker-gene data analysis. ISME J. 11, 2639–2643. https://doi.org/10.1038/ismej.2017.119

Callahan, B.J., McMurdie, P.J., Rosen, M.J., Han, A.W., Johnson, A.J.A., Holmes, S.P., 2016. DADA2: High resolution sample inference from Illumina amplicon data. Nat. Methods 13, 581–583. https://doi.org/10.1038/nmeth.3869

Caporaso, J.G., Lauber, C.L., Walters, W.A., Berg-Lyons, D., Lozupone, C.A., Turnbaugh, P.J., Fierer, N., Knight, R., 2011. Global patterns of 16S rRNA diversity at a depth of millions of sequences per sample. Proc. Natl. Acad. Sci. 108, 4516–4522. https://doi.org/10.1073/pnas.1000080107

Carreira, C., Lønborg, C., Kühl, M., Lillebø, A., Sandaa, R.-A., Villanueva, L., Cruz, S., 2020. Fungi and viruses as important players in microbial mats. FEMS Microbiol. Ecol. 96. https://doi.org/10.1093/femsec/fiaa187

Chakraborty, J., Rajput, V., Sapkale, V., Kamble, S., Dharne, M., 2021. Spatio-temporal resolution of taxonomic and functional microbiome of Lonar soda lake of India reveals metabolic potential for bioremediation. Chemosphere 264, 128574. https://doi.org/10.1016/j.chemosphere.2020.128574

Chen, D.-D., Tian, Y., Jiao, J.-Y., Zhang, X.-T., Zhang, Y.-G., Dong, Z.-Y., Xiong, M.-J., Xiao, M., Shu, W.-S., Li, W.-J., 2020. Comparative genomics analysis of Nitriliruptoria reveals the genomic differences and salt adaptation strategies. Extremophiles 24, 249–264. https://doi.org/10.1007/s00792-019-01150-3

Chen, L., Liu, J., Hu, W., Gao, J., Yang, J., 2021. Vanadium in soil-plant system: Source, fate, toxicity, and bioremediation. J. Hazard. Mater. 405, 124200. https://doi.org/10.1016/j.jhazmat.2020.124200

Chidambaram, D., Hennebel, T., Taghavi, S., Mast, J., Boon, N., Verstraete, W., van der Lelie, D., Fitts, J.P., 2010. Concomitant microbial generation of palladium nanoparticles and hydrogen to immobilize chromate. Environ. Sci. Technol. 44, 7635–7640. https://doi.org/10.1021/es101559r

852   Ciccazzo, S., Esposito, A., Borruso, L., Brusetti, L., 2016. Microbial communities and
853   primary succession in high altitude mountain environments. Ann. Microbiol. 66, 43–
854   60. https://doi.org/10.1007/s13213-015-1130-1
855   Claros, J., Jiménez, E., Borrás, L., Aguado, D., Seco, A., Ferrer, J., Serralta, J., 2010. Short-
856   term effect of ammonia concentration and salinity on activity of ammonia oxidizing
857   bacteria. Water Sci. Technol. 61, 3008–3016. https://doi.org/10.2166/wst.2010.217
858   Copernicus Climate Change Service Climate Data Store (CDS), 2021. Copernicus Climate
859   Change Service (C3S) (2017): ERA5: Fifth generation of ECMWF atmospheric
860   reanalyses of the global climate. ECMWF.
861   Courtney, R., Harris, J., Pawlett, M., 2014. Microbial Community Composition in a
862   Rehabilitated Bauxite Residue Disposal Area: A Case Study for Improving Microbial
863   Community Composition. Restor. Ecol. 22. https://doi.org/10.1111/rec.12143
864   Csardi, G., Nepusz, T., 2006. The igraph software package for complex network research,
865   InterJournal.
866   Cusack, P.B., Courtney, R., Healy, M.G., O' Donoghue, L.M.T., Ujaczki, É., 2019. An
867   evaluation of the general composition and critical raw material content of bauxite
868   residue in a storage area over a twelve-year period. J. Clean. Prod. 208, 393–401.
869   https://doi.org/10.1016/j.jclepro.2018.10.083
870   Dentoni, V., Grosso, B., Pinna, F., 2021. Experimental Evaluation of PM Emission from Red
871   Mud Basins Exposed to Wind Erosion. Minerals 11, 405.
872   https://doi.org/10.3390/min11040405
873   Dev, S., Sachan, A., Dehghani, F., Ghosh, T., Briggs, B.R., Aggarwal, S., 2020. Mechanisms
874   of biological recovery of rare-earth elements from industrial and electronic wastes: A
875   review. Chem. Eng. J. 397, 124596. https://doi.org/10.1016/j.cej.2020.124596
876   Di Carlo, E., Boullemant, A., Courtney, R., 2020. Ecotoxicological risk assessment of
877   revegetated bauxite residue: Implications for future rehabilitation programmes. Sci.
878   Total Environ. 698, 134344. https://doi.org/10.1016/j.scitotenv.2019.134344
879   Di Carlo, E., Chen, C.R., Haynes, R.J., Phillips, I.R., Courtney, R., 2019. Soil quality and
880   vegetation performance indicators for sustainable rehabilitation of bauxite residue
881   disposal areas: a review. Soil Res. 57, 419. https://doi.org/10.1071/SR18348
882   Doebelin, N., Kleeberg, R., 2015. Profex: a graphical user interface for the Rietveld
883   refinement program BGMN. J. Appl. Crystallogr. 48, 1573–1580.
884   https://doi.org/10.1107/S1600576715014685
885   Dominguez-Benetton, X., Varia, J.C., Pozo, G., Modin, O., Ter Heijne, A., Fransaer, J.,
886   Rabaey, K., 2018. Metal recovery by microbial electro-metallurgy. Prog. Mater. Sci.
887   94, 435–461. https://doi.org/10.1016/j.pmatsci.2018.01.007
888   Economou-Eliopoulos, M., Frei, R., Megremi, I., 2016. Potential leaching of Cr(VI) from
889   laterite mines and residues of metallurgical products (red mud and slag): An
890   integrated approach. J. Geochem. Explor. 162, 40–49.
891   https://doi.org/10.1016/j.gexplo.2015.12.007
892   Egidi, E., Delgado-Baquerizo, M., Plett, J.M., Wang, J., Eldridge, D.J., Bardgett, R.D.,
893   Maestre, F.T., Singh, B.K., 2019. A few Ascomycota taxa dominate soil fungal
894   communities worldwide. Nat. Commun. 10, 2369. https://doi.org/10.1038/s41467-
895   019-10373-z
896   European Commission, 2020. Critical Raw Materials for Strategic Technologies and Sectors
897   in the EU.
898   Evans, K., 2016. The History, Challenges, and New Developments in the Management and
899   Use of Bauxite Residue. J. Sustain. Metall. 2, 316–331.
900   https://doi.org/10.1007/s40831-016-0060-x

901   Ferrenberg, S., O'Neill, S.P., Knelman, J.E., Todd, B., Duggan, S., Bradley, D., Robinson,
902   T., Schmidt, S.K., Townsend, A.R., Williams, M.W., Cleveland, C.C., Melbourne,
903   B.A., Jiang, L., Nemergut, D.R., 2013. Changes in assembly processes in soil
904   bacterial communities following a wildfire disturbance. ISME J. 7, 1102–1111.
905   https://doi.org/10.1038/ismej.2013.11
906   Foreman, C.M., Sattler, B., Mikucki, J.A., Porazinska, D.L., Priscu, J.C., 2007. Metabolic
907   activity and diversity of cryoconites in the Taylor Valley, Antarctica. J. Geophys. Res.
908   Biogeosciences 112. https://doi.org/10.1029/2006JG000358
909   Fourrier, C., Luglia, M., Hennebert, P., Foulon, J., Ambrosi, J.-P., Angeletti, B., Keller, C.,
910   Criquet, S., 2020. Effects of increasing concentrations of unamended and gypsum
911   modified bauxite residues on soil microbial community functions and structure – A
912   mesocosm study. Ecotoxicol. Environ. Saf. 201, 110847.
913   https://doi.org/10.1016/j.ecoenv.2020.110847
914   Fourrier, C., Luglia, M., Keller, C., Hennebert, P., Foulon, J., Ambrosi, J.-P., Angeletti, B.,
915   Criquet, S., 2021. How Raw and Gypsum Modified Bauxite Residues Affect Seed
916   Germination, Enzyme Activities, and Root Development of Sinapis alba. Water. Air.
917   Soil Pollut. 232, 309. https://doi.org/10.1007/s11270-021-05232-x
918   Fox, J., Weisberg, S., 2019. An R Companion to Applied Regression, Third. ed. Sage,
919   Thousand Oaks, CA.
920   Gentzmann, M.C., Schraut, K., Vogel, C., Gäbler, H.-E., Huthwelker, T., Adam, C., 2021.
921   Investigation of scandium in bauxite residues of different origin. Appl. Geochem.
922   126, 104898. https://doi.org/10.1016/j.apgeochem.2021.104898
923   Gerea, A.L., Branscum, K.M., King, J.B., You, J., Powell, D.R., Miller, A.N., Spear, J.R.,
924   Cichewicz, R.H., 2012. Secondary metabolites produced by fungi derived from a
925   microbial mat encountered in an iron-rich natural spring. Tetrahedron Lett. 53, 4202–
926   4205. https://doi.org/10.1016/j.tetlet.2012.05.156
927   Ghosh, S., Bal, B., Das, A.P., 2018. Enhancing Manganese Recovery from Low-Grade Ores
928   by Using Mixed Culture of Indigenously Isolated Bacterial Strains. Geomicrobiol. J.
929   35, 242–246. https://doi.org/10.1080/01490451.2017.1362080
930   Gonzalez-Pimentel, J.L., Miller, A.Z., Jurado, V., Laiz, L., Pereira, M.F.C., Saiz-Jimenez, C.,
931   2018. Yellow coloured mats from lava tubes of La Palma (Canary Islands, Spain) are
932   dominated by metabolically active Actinobacteria. Sci. Rep. 8, 1944.
933   https://doi.org/10.1038/s41598-018-20393-2
934   Grum-Grzhimaylo, A.A., Georgieva, M.L., Bondarenko, S.A., Debets, A.J.M., Bilanenko,
935   E.N., 2016. On the diversity of fungi from soda soils. Fungal Divers. 76, 27–74.
936   https://doi.org/10.1007/s13225-015-0320-2
937   Gunde-Cimerman, N., Plemenitaš, A., Oren, A., 2018. Strategies of adaptation of
938   microorganisms of the three domains of life to high salt concentrations. FEMS
939   Microbiol. Rev. 42, 353–375. https://doi.org/10.1093/femsre/fuy009
940   Guo, Y., Fujimura, R., Sato, Y., Suda, W., Kim, S., Oshima, K., Hattori, M., Kamijo, T.,
941   Narisawa, K., Ohta, H., 2014. Characterization of Early Microbial Communities on
942   Volcanic Deposits along a Vegetation Gradient on the Island of Miyake, Japan.
943   Microbes Environ. 29, 38–49. https://doi.org/10.1264/jsme2.ME13142
944   Harantová, L., Mudrák, O., Kohout, P., Elhottová, D., Frouz, J., Baldrian, P., 2017.
945   Development of microbial community during primary succession in areas degraded
946   by mining activities. Land Degrad. Dev. 28, 2574–2584.
947   https://doi.org/10.1002/ldr.2817
948   Herbst, D.B., 1998. Potential salinity limitations on nitrogen fixation in sediments from
949   Mono Lake, California. Int. J. Salt Lake Res. 7, 261–274.
950   https://doi.org/10.1007/BF02441878

Hill, T.C.J., Walsh, K.A., Harris, J.A., Moffett, B.F., 2003. Using ecological diversity measures with bacterial communities. FEMS Microbiol. Ecol. 43, 1–11. https://doi.org/10.1111/j.1574-6941.2003.tb01040.x

Hingole, S., Pathak, A., 2013. Report on efficient salt stable Azospirillum a Lonar Soda Lake isolate. Sci. Res. Report. 3, 200–203.

Hodkinson, I.D., Webb, N.R., Coulson, S.J., 2002. Primary community assembly on land – the missing stages: why are the heterotrophic organisms always there first? J. Ecol. 90, 569–577. https://doi.org/10.1046/j.1365-2745.2002.00696.x

Ihrmark, K., Bödeker, I.T.M., Cruz-Martinez, K., Friberg, H., Kubartova, A., Schenck, J., Strid, Y., Stenlid, J., Brandström-Durling, M., Clemmensen, K.E., Lindahl, B.D., 2012. New primers to amplify the fungal ITS2 region – evaluation by 454-sequencing of artificial and natural communities. FEMS Microbiol. Ecol. 82, 666–677. https://doi.org/10.1111/j.1574-6941.2012.01437.x

International Aluminium Institute (IAI), European Aluminium (EA), 2015. Bauxite Residue Management: Best Practice [WWW Document]. URL www.world-aluminium.org

Jamieson, J., Prommer, H., Kaksonen, A.H., Sun, J., Siade, A.J., Yusov, A., Bostick, B., 2018. Identifying and Quantifying the Intermediate Processes during Nitrate-Dependent Iron(II) Oxidation. Environ. Sci. Technol. 52, 5771–5781. https://doi.org/10.1021/acs.est.8b01122

Ji, M., Kong, W., Yue, L., Wang, J., Deng, Y., Zhu, L., 2019. Salinity reduces bacterial diversity, but increases network complexity in Tibetan Plateau lakes. FEMS Microbiol. Ecol. 95. https://doi.org/10.1093/femsec/fiz190

Jones, B.E.H., Haynes, R.J., Phillips, I.R., 2011. Influence of organic waste and residue mud additions on chemical, physical and microbial properties of bauxite residue sand. Environ. Sci. Pollut. Res. 18, 199–211. https://doi.org/10.1007/s11356-010-0364-5

Jones, R.T., Robeson, M.S., Lauber, C.L., Hamady, M., Knight, R., Fierer, N., 2009. A comprehensive survey of soil acidobacterial diversity using pyrosequencing and clone library analyses. ISME J. 3, 442–453. https://doi.org/10.1038/ismej.2008.127

Kalwasińska, A., Felföldi, T., Szabó, A., Deja-Sikora, E., Kosobucki, P., Walczak, M., 2017. Microbial communities associated with the anthropogenic, highly alkaline environment of a saline soda lime, Poland. Antonie Van Leeuwenhoek 110, 945–962. https://doi.org/10.1007/s10482-017-0866-y

Kalwasińska, A., Jankiewicz, U., Felföldi, T., Burkowska-But, A., Brzezinska, M.S., 2018. Alkaline and Halophilic Protease Production by Bacillus luteus H11 and Its Potential Industrial Applications. Food Technol. Biotechnol. 56, 553–561. https://doi.org/10.17113/ftb.56.04.18.5553

Kassambara, A., 2021. rstatix: Pipe-Friendly Framework for Basic Statistical Tests.

Kassambara, A., 2020. ggpubr: "ggplot2" Based Publication Ready Plots.

Kassambara, A., Mundt, F., 2020. factoextra: Extract and Visualize the Results of Multivariate Data Analyses.

Ke, W., 2021. Appropriate human intervention stimulates the development of microbial communities and soil formation at a long-term weathered bauxite residue disposal area. J. Hazard. Mater. 10.

Khaitan, S., Dzombak, D.A., Swallow, P., Schmidt, K., Fu, J., Lowry, G.V., 2010. Field Evaluation of Bauxite Residue Neutralization by Carbon Dioxide, Vegetation, and Organic Amendments. J. Environ. Eng. 136, 1045–1053. https://doi.org/10.1061/(ASCE)EE.1943-7870.0000230

Kielak, A.M., Barreto, C.C., Kowalchuk, G.A., van Veen, J.A., Kuramae, E.E., 2016. The Ecology of Acidobacteria: Moving beyond Genes and Genomes. Front. Microbiol. 7. https://doi.org/10.3389/fmicb.2016.00744

Kim, Y.M., Park, H., Chandran, K., 2016. Nitrification inhibition by hexavalent chromium Cr(VI) – Microbial ecology, gene expression and off-gas emissions. Water Res. 92, 254–261. https://doi.org/10.1016/j.watres.2016.01.042

Kiskira, K., Lymperopoulou, T., Tsakanika, L.-A., Pavlopoulos, C., Papadopoulou, K., Ochsenkühn, K.-M., Lyberatos, G., Ochsenkühn-Petropoulou, M., 2021. Study of Microbial Cultures for the Bioleaching of Scandium from Alumina Industry By-Products. Metals 11, 951. https://doi.org/10.3390/met11060951

Krishna, P., Babu, A.G., Reddy, M.S., 2014. Bacterial diversity of extremely alkaline bauxite residue site of alumina industrial plant using culturable bacteria and residue 16S rRNA gene clones 12.

Kumaraswamy, R., Sjollema, K., Kuenen, J.G., van Loosdrecht, M., Muyzer, G., 2006. Paracoccus ferroxidans.

Lê, S., Josse, J., Husson, F., 2008. FactoMineR: An R Package for Multivariate Analysis. J. Stat. Softw. 25. https://doi.org/10.18637/jss.v025.i01

Levard, C., Borschneck, D., Grauby, O., Rose, J., Ambrosi, J.P., 2018. Goethite, a tailor-made host for the critical metal scandium: The FexSc(1-x)OOH solid solution. Geochem. Perspect. Lett. 9, 16–20. https://doi.org/10.7185/geochemlet.1832

Li, K., Liu, R., Zhang, H., Yun, J., 2013. The Diversity and Abundance of Bacteria and Oxygenic Phototrophs in Saline Biological Desert Crusts in Xinjiang, Northwest China. Microb. Ecol. 66, 40–48. https://doi.org/10.1007/s00248-012-0164-1

Liang, J., Huang, X., Yan, J., Li, Y., Zhao, Z., Liu, Y., Ye, J., Wei, Y., 2021. A review of the formation of Cr(VI) via Cr(III) oxidation in soils and groundwater. Sci. Total Environ. 774, 145762. https://doi.org/10.1016/j.scitotenv.2021.145762

Litchfield, C.D., 2011. Potential for industrial products from the halophilic Archaea. J. Ind. Microbiol. Biotechnol. 38, 1635–1635. https://doi.org/10.1007/s10295-011-1021-9

Lozupone, C.A., Hamady, M., Kelley, S.T., Knight, R., 2007. Quantitative and Qualitative β Diversity Measures Lead to Different Insights into Factors That Structure Microbial Communities. Appl. Environ. Microbiol. 73, 1576–1585. https://doi.org/10.1128/AEM.01996-06

Lyu, F., Hu, Y., Wang, L., Sun, W., 2021. Dealkalization processes of bauxite residue: A comprehensive review. J. Hazard. Mater. 403, 123671. https://doi.org/10.1016/j.jhazmat.2020.123671

Ma, L., Wang, H., Wu, J., Wang, Y., Zhang, D., Liu, X., 2019. Metatranscriptomics reveals microbial adaptation and resistance to extreme environment coupling with bioleaching performance. Bioresour. Technol. 280, 9–17. https://doi.org/10.1016/j.biortech.2019.01.117

Ma, L., Wang, X., Feng, X., Liang, Y., Xiao, Y., Hao, X., Yin, H., Liu, H., Liu, X., 2017. Co-culture microorganisms with different initial proportions reveal the mechanism of chalcopyrite bioleaching coupling with microbial community succession. Bioresour. Technol. 223, 121–130. https://doi.org/10.1016/j.biortech.2016.10.056

Maes, S., Claus, M., Verbeken, K., Wallaert, E., De Smet, R., Vanhaecke, F., Boon, N., Hennebel, T., 2016. Platinum recovery from industrial process streams by halophilic bacteria: Influence of salt species and platinum speciation. Water Res. 105, 436–443. https://doi.org/10.1016/j.watres.2016.09.023

Maharaja, P., Nanthini, E., Swarnalatha, S., Sekaran, G., 2018. Studies on the Production of Salt-Tolerant Alkaline Protease Isolated from Proteus mirabilis and Its Degradation of Hyper-Saline Soak Liquor, in: Singh, V.P., Yadav, S., Yadava, R.N. (Eds.), Environmental Pollution, Water Science and Technology Library. Springer, Singapore, pp. 439–457. https://doi.org/10.1007/978-981-10-5792-2_35

Maleke, M., Valverde, A., Gomez-Arias, A., Cason, E.D., Vermeulen, J.-G., Coetsee-Hugo, L., Swart, H., van Heerden, E., Castillo, J., 2019. Anaerobic reduction of europium by a Clostridium strain as a strategy for rare earth biorecovery. Sci. Rep. 9, 14339. https://doi.org/10.1038/s41598-019-50179-z

Mamo, G., 2020. Challenges and Adaptations of Life in Alkaline Habitats, in: Mamo, G., Mattiasson, B. (Eds.), Alkaliphiles in Biotechnology, Advances in Biochemical Engineering/Biotechnology. Springer International Publishing, Cham, pp. 85–133. https://doi.org/10.1007/10_2019_97

Markus Gräfe, Matthew Landers, Ryan Tappero, Peter Austin, Bee Gan, Alton Grabsch, Craig Klauber, 2011. Combined Application of QEM-SEM and Hard X-ray Microscopy to Determine Mineralogical Associations and Chemical Speciation of Trace Metals. J. Environ. Qual. https://doi.org/10.2134/jeq2010.0214

Maza-Márquez, P., Lee, M.D., Bebout, B.M., 2021. The Abundance and Diversity of Fungi in a Hypersaline Microbial Mat from Guerrero Negro, Baja California, México. J. Fungi Basel Switz. 7, 210. https://doi.org/10.3390/jof7030210

McDonald, D., Price, M.N., Goodrich, J., Nawrocki, E.P., DeSantis, T.Z., Probst, A., Andersen, G.L., Knight, R., Hugenholtz, P., 2012. An improved Greengenes taxonomy with explicit ranks for ecological and evolutionary analyses of bacteria and archaea. ISME J. 6, 610–618. https://doi.org/10.1038/ismej.2011.139

Meng, C., Kuster, B., Culhane, A.C., Gholami, A.M., 2014. A multivariate approach to the integration of multi-omics datasets. BMC Bioinformatics 15, 162. https://doi.org/10.1186/1471-2105-15-162

Milačič, R., Zuliani, T., Ščančar, J., 2012. Environmental impact of toxic elements in red mud studied by fractionation and speciation procedures. Sci. Total Environ. 426, 359–365. https://doi.org/10.1016/j.scitotenv.2012.03.080

Muller, L.A.H., Ballhausen, M.-B., Andrade-Linares, D.R., Pinek, L., Golubeva, P., Rillig, M.C., 2021. Fungus–bacterium associations are widespread in fungal cultures isolated from a semi-arid natural grassland in Germany. FEMS Microbiol. Ecol. 97, fiab059. https://doi.org/10.1093/femsec/fiab059

Muyzer, G., de Waal, E.C., Uitterlinden, A.G., 1993. Profiling of complex microbial populations by denaturing gradient gel electrophoresis analysis of polymerase chain reaction-amplified genes coding for 16S rRNA. Appl. Environ. Microbiol. 59, 695–700.

Navarro-Noya, Y.E., Luna-Guido, M., Dendooven, L., 2016. Cultivable Nitrogen Fixing Bacteria from Extremely Alkaline-Saline Soils. Adv. Microbiol. 6, 412–423. https://doi.org/10.4236/aim.2016.66041

Ohlsson, J.I., Osvatic, J.T., Becraft, E.D., Swingley, W.D., 2019. Microbial Community in Hyperalkaline Steel Slag-Fill Emulates Serpentinizing Springs. Diversity 11, 103. https://doi.org/10.3390/d11070103

Oksanen, J., Blanchet, F.G., Friendly, M., Kindt, R., Legendre, P., McGlinn, D., Minchin, P.R., O'Hara, R.B., Simpson, G.L., Solymos, P., Stevens, M.H.H., Szoecs, E., Wagner, H., 2020. vegan: Community Ecology Package.

Oliveira, A., Pampulha, M.E., 2006. Effects of long-term heavy metal contamination on soil microbial characteristics. J. Biosci. Bioeng. 102, 157–161. https://doi.org/10.1263/jbb.102.157

Ollivier, J., Töwe, S., Bannert, A., Hai, B., Kastl, E.-M., Meyer, A., Su, M.X., Kleineidam, K., Schloter, M., 2011. Nitrogen turnover in soil and global change. FEMS Microbiol. Ecol. 78, 3–16. https://doi.org/10.1111/j.1574-6941.2011.01165.x

Ortiz-Álvarez, R., Fierer, N., de los Ríos, A., Casamayor, E.O., Barberán, A., 2018. Consistent changes in the taxonomic structure and functional attributes of bacterial

communities during primary succession. ISME J. 12, 1658–1667.
https://doi.org/10.1038/s41396-018-0076-2

Panda, S., Costa, R.B., Shah, S.S., Mishra, S., Bevilaqua, D., Akcil, A., 2021.
Biotechnological trends and market impact on the recovery of rare earth elements
from bauxite residue (red mud) – A review. Resour. Conserv. Recycl. 171, 105645.
https://doi.org/10.1016/j.resconrec.2021.105645

Perez-Garcia, O., Lear, G., Singhal, N., 2016. Metabolic Network Modeling of Microbial
Interactions in Natural and Engineered Environmental Systems. Front. Microbiol. 7.
https://doi.org/10.3389/fmicb.2016.00673

Poudel, R., Jumpponen, A., Schlatter, D.C., Paulitz, T.C., Gardener, B.B.M., Kinkel, L.L.,
Garrett, K.A., 2016. Microbiome Networks: A Systems Framework for Identifying
Candidate Microbial Assemblages for Disease Management. Phytopathology® 106,
1083–1096. https://doi.org/10.1094/PHYTO-02-16-0058-FI

Presentato, A., Piacenza, E., Turner, R.J., Zannoni, D., Cappelletti, M., 2020. Processing of
Metals and Metalloids by Actinobacteria: Cell Resistance Mechanisms and Synthesis
of Metal(loid)-Based Nanostructures. Microorganisms 8, 2027.
https://doi.org/10.3390/microorganisms8122027

Qiu, L., Zhang, Q., Zhu, H., Reich, P.B., Banerjee, S., van der Heijden, M.G.A., Sadowsky,
M.J., Ishii, S., Jia, X., Shao, M., Liu, B., Jiao, H., Li, H., Wei, X., 2021. Erosion
reduces soil microbial diversity, network complexity and multifunctionality. ISME J.
15, 2474–2489. https://doi.org/10.1038/s41396-021-00913-1

Qu, Y., Li, H., Wang, X., Tian, W., Shi, B., Yao, M., Zhang, Y., 2019. Bioleaching of Major,
Rare Earth, and Radioactive Elements from Red Mud by using Indigenous
Chemoheterotrophic Bacterium Acetobacter sp. Minerals 9, 67.
https://doi.org/10.3390/min9020067

R Core Team, 2020. R: A language and environment for statistical computing. R Foundation
for Statistical Computing, Vienna, Austria.

Ren, J., Chen, J., Han, L., Wang, M., Yang, B., Du, P., Li, F., 2018. Spatial distribution of
heavy metals, salinity and alkalinity in soils around bauxite residue disposal area. Sci.
Total Environ. 628–629, 1200–1208. https://doi.org/10.1016/j.scitotenv.2018.02.149

Rivera, R.M., Ounoughene, G., Malfliet, A., Vind, J., Panias, D., Vassiliadou, V.,
Binnemans, K., Van Gerven, T., 2019. A Study of the Occurrence of Selected Rare-
Earth Elements in Neutralized–Leached Bauxite Residue and Comparison with
Untreated Bauxite Residue. J. Sustain. Metall. 5, 57–68.
https://doi.org/10.1007/s40831-018-0206-0

Roy, A., Dutta, A., Pal, S., Gupta, A., Sarkar, J., Chatterjee, A., Saha, A., Sarkar, P., Sar, P.,
Kazy, S.K., 2018. Biostimulation and bioaugmentation of native microbial
community accelerated bioremediation of oil refinery sludge. Bioresour. Technol.
253, 22–32. https://doi.org/10.1016/j.biortech.2018.01.004

Sajjad, W., Zheng, G., Ma, X., Xu, W., Ali, B., Rafiq, M., Zada, S., Irfan, M., Zeman, J.,
2020. Dissolution of Cu and Zn-bearing ore by indigenous iron-oxidizing bacterial
consortia supplemented with dried bamboo sawdust and variations in bacterial
structural dynamics: A new concept in bioleaching. Sci. Total Environ. 709, 136136.
https://doi.org/10.1016/j.scitotenv.2019.136136

Salano, O.A., Makonde, H.M., Kasili, R.W., Wangai, L.N., Nawiri, M.P., Boga, H.I., 2017.
Diversity and distribution of fungal communities within the hot springs of soda lakes
in the Kenyan rift valley. Afr. J. Microbiol. Res. 11, 764–775.
https://doi.org/10.5897/AJMR2017.8510

Santini, T., Kerr, J.L., Warren, L.A., 2015a. Microbially-driven strategies for bioremediation of bauxite residue. J. Hazard. Mater. 293, 131–157. https://doi.org/10.1016/j.jhazmat.2015.03.024

Santini, T., Warren, L.A., Kendra, K.E., 2015b. Microbial Diversity in Engineered Haloalkaline Environments Shaped by Shared Geochemical Drivers Observed in Natural Analogues. Appl. Environ. Microbiol. 81, 5026–5036. https://doi.org/10.1128/AEM.01238-15

Santini, T.C., Malcolm, L.I., Tyson, G.W., Warren, L.A., 2016. pH and Organic Carbon Dose Rates Control Microbially Driven Bioremediation Efficacy in Alkaline Bauxite Residue. Environ. Sci. Technol. 50, 11164–11173. https://doi.org/10.1021/acs.est.6b01973

Santini, T.C., Wang, J.C., Warren, K.L., Pickering, G., Raudsepp, M.J., 2021. Simple Organic Carbon Sources and High Diversity Inocula Enhance Microbial Bioneutralization of Alkaline Bauxite Residues. Environ. Sci. Technol. 55, 3929–3939. https://doi.org/10.1021/acs.est.0c02534

Santini, T.C., Warren, K., Raudsepp, M., Carter, N., Hamley, D., McCosker, C., Couperthwaite, S., Southam, G., Tyson, G.W., Warren, L.A., 2019. Accelerating Bauxite Residue Remediation with Microbial Biotechnology, in: Chesonis, C. (Ed.), Light Metals 2019, The Minerals, Metals & Materials Series. Springer International Publishing, Cham, pp. 69–77. https://doi.org/10.1007/978-3-030-05864-7_10

Schmalenberger, A., 2013. Bacterial Communities Established in Bauxite Residues with Different Restoration Histories. Env. Sci Technol 10.

Schmidt, S.K., Nemergut, D.R., Darcy, J.L., Lynch, R., 2014. Do bacterial and fungal communities assemble differently during primary succession? Mol. Ecol. 23, 254–258. https://doi.org/10.1111/mec.12589

Schmidt, S.K., Reed, S.C., Nemergut, D.R., Stuart Grandy, A., Cleveland, C.C., Weintraub, M.N., Hill, A.W., Costello, E.K., Meyer, A.F., Neff, J.C., Martin, A.M., 2008. The earliest stages of ecosystem succession in high-elevation (5000 metres above sea level), recently deglaciated soils. Proc. R. Soc. B Biol. Sci. 275, 2793–2802. https://doi.org/10.1098/rspb.2008.0808

Segata, N., Izard, J., Waldron, L., Gevers, D., Miropolsky, L., Garrett, W.S., Huttenhower, C., 2011. Metagenomic biomarker discovery and explanation. Genome Biol. 12, R60. https://doi.org/10.1186/gb-2011-12-6-r60

Shameer, S., 2016. Haloalkaliphilic Bacillus species from solar salterns: an ideal prokaryote for bioprospecting studies. Ann. Microbiol. 66, 1315–1327. https://doi.org/10.1007/s13213-016-1221-7

Shivlata, L., Tulasi, S., 2015. Thermophilic and alkaliphilic Actinobacteria: biology and potential applications. Front. Microbiol. 6. https://doi.org/10.3389/fmicb.2015.01014

Srichandan, H., Mohapatra, R.K., Parhi, P.K., Mishra, S., 2019. Bioleaching approach for extraction of metal values from secondary solid wastes: A critical review. Hydrometallurgy 189, 105122. https://doi.org/10.1016/j.hydromet.2019.105122

Straub, K.L., Benz, M., Schink, B., Widdel, F., 1996. Anaerobic, nitrate-dependent microbial oxidation of ferrous iron. Appl. Environ. Microbiol. 62, 1458–1460. https://doi.org/10.1128/aem.62.4.1458-1460.1996

Sun, W., Xiao, E., Häggblom, M., Krumins, V., Dong, Y., Sun, X., Li, F., Wang, Q., Li, B., Yan, B., 2018. Bacterial Survival Strategies in an Alkaline Tailing Site and the Physiological Mechanisms of Dominant Phylotypes As Revealed by Metagenomic Analyses. Environ. Sci. Technol. 52, 13370–13380. https://doi.org/10.1021/acs.est.8b03853

Tian, T., Liu, Z., Zhu, F., Hartley, W., Ye, Y., Xue, S., 2020. Improvement of aggregate-associated organic carbon and its stability in bauxite residue by substrate amendment addition. Land Degrad. Dev. 31, 2405–2416. https://doi.org/10.1002/ldr.3609

Ujaczki, É., Zimmermann, Y., Gasser, C., Molnár, M., Feigl, V., Lenz, M., 2017. Red mud as secondary source for critical raw materials - purification of rare earth elements by liquid/liquid extraction: Red mud as secondary source for critical raw materials. J. Chem. Technol. Biotechnol. 92, 2683–2690. https://doi.org/10.1002/jctb.5289

Vaidya, S., Dev, K., Sourirajan, A., 2018. Distinct Osmoadaptation Strategies in the Strict Halophilic and Halotolerant Bacteria Isolated from Lunsu Salt Water Body of North West Himalayas. Curr. Microbiol. 75, 888–895. https://doi.org/10.1007/s00284-018-1462-8

Vind, J., Malfliet, A., Blanpain, B., Tsakiridis, P., Tkaczyk, A., Vassiliadou, V., Panias, D., 2018. Rare Earth Element Phases in Bauxite Residue. Minerals 8, 77. https://doi.org/10.3390/min8020077

Wagg, C., Schlaeppi, K., Banerjee, S., Kuramae, E.E., van der Heijden, M.G.A., 2019. Fungal-bacterial diversity and microbiome complexity predict ecosystem functioning. Nat. Commun. 10, 4841. https://doi.org/10.1038/s41467-019-12798-y

Wang, L., Yin, S., Wu, A., Chen, W., 2020. Synergetic bioleaching of copper sulfides using mixed microorganisms and its community structure succession. J. Clean. Prod. 245, 118689. https://doi.org/10.1016/j.jclepro.2019.118689

Wang, M., Chen, S., Chen, L., Wang, D., 2019. Responses of soil microbial communities and their network interactions to saline-alkaline stress in Cd-contaminated soils. Environ. Pollut. 252, 1609–1621. https://doi.org/10.1016/j.envpol.2019.06.082

Wee, S.K., Burns, J.L., DiChristina, T.J., 2014. Identification of a molecular signature unique to metal-reducing Gammaproteobacteria. FEMS Microbiol. Lett. 350, 90–99. https://doi.org/10.1111/1574-6968.12304

Wickham, H., 2009. ggplot2: Elegant Graphics for Data Analysis, 2197-5736. Springer-Verlag, New York, NY.

Wickham, H., François, R., Henry, L., Müller, K., 2021. dplyr: A Grammar of Data Manipulation.

Williams, R.J., Howe, A., Hofmockel, K.S., 2014. Demonstrating microbial co-occurrence pattern analyses within and between ecosystems. Front. Microbiol. 5, 358. https://doi.org/10.3389/fmicb.2014.00358

Wong, J.W.C., Ho, G., 1994. Sewage sludge as organic ameliorant for revegetation of fine bauxite refining residue. Resour. Conserv. Recycl., Environmental biotechnology in waste treatment and recycling 11, 297–309. https://doi.org/10.1016/0921-3449(94)90097-3

World Aluminium, 2020. World Aluminium [WWW Document]. URL www.world-aluminium.org (accessed 6.8.21).

Wu, H., Chen, L., Zhu, F., Hartley, W., Zhang, Y., Xue, S., 2020. The dynamic development of bacterial community following long-term weathering of bauxite residue. J. Environ. Sci. 90, 321–330. https://doi.org/10.1016/j.jes.2019.12.001

Wu, H., Liao, J., Zhu, F., Millar, G., Courtney, R., Xue, S., 2019. Isolation of an acid producing Bacillus sp. EEEL02: Potential for bauxite residue neutralization. J. Cent. South Univ. 26, 343–352. https://doi.org/10.1007/s11771-019-4006-x

Wu, H., Tang, T., Zhu, F., Wei, X., Hartley, W., Xue, S., 2021. Long term natural restoration creates soil-like microbial communities in bauxite residue: A 50-year filed study. Land Degrad. Dev. 32, 1606–1617. https://doi.org/10.1002/ldr.3728

1245 X. Kong, Guo, Y., Xue, S., Hartley, W., Wu, C., Ye, Y., Cheng, Q., 2017. Natural evolution
1246   of alkaline characteristics in bauxite residue. J. Clean. Prod. 143, 224–230.
1247   https://doi.org/10.1016/j.jclepro.2016.12.125
1248 Xiao, X., Wang, M., Zhu, H., Guo, Z., Han, X., Zeng, P., 2017. Response of soil microbial
1249   activities and microbial community structure to vanadium stress. Ecotoxicol. Environ.
1250   Saf. 142, 200–206. https://doi.org/10.1016/j.ecoenv.2017.03.047
1251 Xue, S., Zhu, F., Kong, X., Wu, C., Huang, L., Huang, N., Hartley, W., 2016. A review of the
1252   characterization and revegetation of bauxite residues (Red mud). Environ. Sci. Pollut.
1253   Res. 23, 1120–1132. https://doi.org/10.1007/s11356-015-4558-8
1254 Yuan, Q., Wang, P., Wang, C., Chen, J., Wang, X., Liu, S., 2021. Indicator species and co-
1255   occurrence pattern of sediment bacterial community in relation to alkaline copper
1256   mine drainage contamination. Ecol. Indic. 120, 106884.
1257   https://doi.org/10.1016/j.ecolind.2020.106884
1258 Zech, W., Schad, P., Hintermaier-Erhard, G., 2014. Trockene Subtropen und Tropen, in:
1259   Zech, W., Schad, P., Hintermaier-Erhard, G. (Eds.), Böden der Welt: Ein Bildatlas.
1260   Springer, Berlin, Heidelberg, pp. 68–85. https://doi.org/10.1007/978-3-642-36575-
1261   1_7
1262 Zeng, J., Lou, K., Zhang, C.-J., Wang, J.-T., Hu, H.-W., Shen, J.-P., Zhang, L.-M., Han, L.-
1263   L., Zhang, T., Lin, Q., Chalk, P.M., He, J.-Z., 2016. Primary Succession of Nitrogen
1264   Cycling Microbial Communities Along the Deglaciated Forelands of Tianshan
1265   Mountain, China. Front. Microbiol. 7, 1353.
1266   https://doi.org/10.3389/fmicb.2016.01353
1267 Zhang, D., Chen, H., Nie, Z., Xia, J., Li, E., Fan, X., Zheng, L., 2020. Extraction of Al and
1268   rare earths (Ce, Gd, Sc, Y) from red mud by aerobic and anaerobic bi-stage
1269   bioleaching. Chem. Eng. J. 401, 125914. https://doi.org/10.1016/j.cej.2020.125914
1270 Zhang, K., Shi, Y., Cui, X., Yue, P., Li, K., Liu, X., Tripathi, B.M., Chu, H., 2019. Salinity Is
1271   a Key Determinant for Soil Microbial Communities in a Desert Ecosystem. mSystems
1272   4, e00225-18. https://doi.org/10.1128/mSystems.00225-18
1273 Zhang, Y., Qin, W., Wang, J., Zhen, S., Yang, C., Zhang, J., Nai, S., Qiu, G., 2008.
1274   Bioleaching of chalcopyrite by pure and mixed culture. Trans. Nonferrous Met. Soc.
1275   China 18, 1491–1496. https://doi.org/10.1016/S1003-6326(09)60031-5
1276 Zhu, F., Xue, S., Hartley, W., Huang, L., Wu, C., Li, X., 2016. Novel predictors of soil
1277   genesis following natural weathering processes of bauxite residues. Environ. Sci.
1278   Pollut. Res. 23, 2856–2863. https://doi.org/10.1007/s11356-015-5537-9
1279